

Structured Prediction Cascades

David Weiss, Benjamin Sapp, Ben Taskar
 djweiss@cis.upenn.edu, bensapp@cis.upenn.edu, taskar@cis.upenn.edu

Department of Computer and Information Science
 University of Pennsylvania
 Philadelphia, PA 19104-6309, USA

August 17, 2012

Abstract

Structured prediction tasks pose a fundamental trade-off between the need for model complexity to increase predictive power and the limited computational resources for inference in the exponentially-sized output spaces such models require. We formulate and develop the *Structured Prediction Cascade* architecture: a sequence of increasingly complex models that progressively filter the space of possible outputs. The key principle of our approach is that each model in the cascade is optimized to accurately filter and refine the structured output state space of the *next* model, speeding up both learning and inference in the next layer of the cascade. We learn cascades by optimizing a novel convex loss function that controls the trade-off between the filtering efficiency and the accuracy of the cascade, and provide generalization bounds for both accuracy and efficiency. We also extend our approach to intractable models using tree-decomposition ensembles, and provide algorithms and theory for this setting. We evaluate our approach on several large-scale problems, achieving state-of-the-art performance in handwriting recognition and human pose recognition. We find that structured prediction cascades allow tremendous speedups and the use of previously intractable features and models in both settings.

1 Introduction

The classical trade-off between approximation and estimation error (bias/variance) is fundamental in machine learning. In regression and classification problems, the *approximation error* can be reduced by increasing the complexity of the model at the cost of higher *estimation error*. Standard statistical model selection techniques (Mallows, 1973; Vapnik and Chervonenkis, 1974; Akaike, 1974; Devroye et al., 1996; Barron et al., 1999; Bartlett et al., 2002) explore a hierarchy of models of increasing complexity primarily to minimize expected error, without much concern for the computational cost of using the model at test time.

However, in structured prediction tasks, such as machine translation, speech recognition, articulated human pose estimation and many other complex prediction problems, *test-time computational constraints* play a critical role as models with increasing inference complexity are considered. In these tasks, there is an exponential number of possible predictions for every input. Breaking these joint predictions up into independent decisions (e.g., translate each word independently, recognize a phoneme at a time, detect arms separately) ignores critical correlations and leads to poor performance. On the other hand, structured models used for these tasks, such as grammars and graphical models, can capture strong dependencies but at considerable cost of inference. For example, a first

order conditional random field (CRF) (Lafferty et al., 2001) is fast to evaluate but may not be an accurate model for phoneme recognition, while a fifth order model is more accurate, but prohibitively expensive for both learning and prediction. Model complexity can of course also lead to over-fitting problems due to the sparseness of the training data, but this aspect of the error is fairly well understood and controlled using standard regularization and feature selection methods.

In practice, model complexity is limited by computational constraints at prediction time, either explicitly by the user or implicitly because of the limits of available computation power. We therefore need to balance *inference error* with *inference efficiency*. A common solution is to use heuristic pruning techniques or approximate search methods in order to make more complex models feasible. For example, in statistical machine translation, syntactic models are combined with n-gram language models to produce impractically large inference problems, which are heavily and heuristically pruned in order to fit into memory and any reasonable time budget (Chiang et al., 2005; Venugopal et al., 2007; Petrov et al., 2008). However, previous work remains unsatisfactory in several respects: (1) model parameters are not learned specifically to balance the accuracy/efficiency trade-off, but instead using remotely related criteria, and (2) no optimality or generalization guarantees exist.

In this paper, we address the accuracy/efficiency trade-off for structured problems by learning a *cascade* of structured prediction models, in which the input is passed through a sequence of models of increasing computational complexity before a final prediction is produced. The key principle of our approach is that each model in the cascade is optimized to accurately filter and refine the structured output state space of the *next* model, speeding up both learning and inference in the next layer of the cascade. Although complexity of inference increases (perhaps exponentially) from one layer to the next, the *state-space sparsity* of inference increases exponentially as well, and the entire cascade procedure remains highly efficient. We call our approach *Structured Prediction Cascades* (SPC).

The contributions of this paper are organized as follows.¹

- In Section 3, we describe the SPC inference framework for tree-structured problems where sparse exact inference is tractable. We also propose a tree-decomposition method for applying cascades to loopy graphical models in Section 3.2.
- In Section 4, we describe how cascades can be learned to achieve a desired accuracy/efficiency trade-off on training data. We introduce a novel convex loss function specifically geared for learning to filter accurately and effectively, and describe a simple stochastic subgradient algorithm for learning a cascade one layer at a time.
- In Section 5, we provide a theoretical analysis of the accuracy/efficiency trade-off of the cascade. We develop novel generalization bounds for both *accuracy and efficiency* of a structured prediction model.
- In Section 6, we explore in depth two applications of the SPC framework in which the cascades achieve best-known performance. In Section 6.1, we show how SPC can be applied to linear-chain models for handwriting recognition. In Section 6.2, we demonstrate the use of SPC for single-frame human pose estimation using a pictorial structures tree model cascade. Finally, in Section 6.3, we show how SPC can be applied to the estimating pose in video, using the framework for loopy graphical models introduced in section 3.2.

¹Preliminary analysis and applications of structured prediction cascade was developed in (Weiss and Taskar, 2010; Sapp et al., 2010b; Weiss et al., 2010).

2 Related Work

The trade-off between computation time and model complexity, which is the central focus of this work, has been studied before in several settings we outline in this section.

Training-time Computation Trade-Offs. Several recent works have considered the trade-off between estimation error and computation (number of examples processed) at *training* time in large-scale classification using stochastic/online optimization methods, notably (Shalev-Shwartz and Srebro, 2008; Bottou and Bousquet, 2008). We use such stochastic sub-gradient methods in our learning procedure (Section 4). In more recent theoretical work, Agarwal et al. (2011) also address the issue of estimation time by incorporating computational constraints into the classical empirical risk minimization framework. However, as above, Agarwal et al. (2011) assume that model selection requires choosing between different methods with fixed test-time computational cost for all examples. In this paper, we instead analyze adaptive computational trade-offs in structured inference at test-time, and analyze the trade-offs in terms of novel loss functions measuring efficiency and accuracy.

Test-time Computation Trade-Offs. The issue of controlling computation at test-time also comes up in kernelized classifiers, where prediction speed depends on the number of “support vectors”. Several algorithms, including the Forgetron and Randomized Budget Perceptron (Crammer et al., 2003; Dekel et al., 2008; Cavallanti et al., 2007), are designed to maintain a limited active set of support vectors in an online fashion while minimizing error. However, unlike our approach, these algorithms learn a model that has a fixed running time for each test example. In contrast, our approach addresses structured prediction problems and has a *example-adaptive* computational cost that allows for more computation time on more difficult examples, and greater efficiency gains on examples where simpler models suffice.

Cascades/Coarse-to-fine reasoning. For binary classification, cascades of classifiers have been quite successful for reducing computation. Fleuret and Geman (2001) propose a coarse-to-fine sequence of binary tests to detect the presence and pose of objects in an image. The learned sequence of tests is trained to minimize expected computational cost. The extremely popular classifier of Viola and Jones (2001) implements a cascade of boosting ensembles, with earlier stages using fewer features to quickly reject large portions of the state space. More recent work on binary classification cascades has focused on further increasing efficiency, e.g. through joint optimization (Lefakis and Fleuret, 2010) or selecting features at test time (Gao and Koller, 2011). Our cascade framework is inspired by these binary classification cascades, but poses new objectives, inference, and learning algorithms, to deal with the structured inference setting.

In natural language parsing, several works (Charniak, 2000; Carreras. et al., 2008; Petrov, 2009) use a coarse-to-fine idea closely related to ours and Fleuret and Geman (2001): the marginals of a simple context free grammar or dependency model are used to prune the parse chart for a more complex grammar. We compare to this idea in our experiments. The key difference with our work is that we explicitly learn a sequence of models tuned specifically to filter the space accurately and effectively. Unlike the work of Petrov (2009), however, we do not learn the structure of the hierarchy of models but assume it is given by the designer. Rush and Petrov (2012) apply the ideas developed in our preliminary work to the problem of dependency parsing in natural language processing. Rush and Petrov (2012) learn a cascade of simplified parsing models using the objective presented in section 4 to achieve state-of-the-art performance in dependency parsing across several languages at about two orders of magnitude less time.

Felzenszwalb et al. (2010) proposed a cascade for a structured parts-based object detection model. Their cascade works by early stopping while evaluating individual parts, if the combined part scores are less than fixed thresholds. While the form of this cascade can be posed in our more general framework (a cascade of models with an increasing number of parts), we differ from Felzenszwalb et al. (2010) in that our pruning is based on thresholds that adapt based on inference in each test example, and we explicitly learn parameters in order to prune safely and efficiently. In Fleuret and Geman (2001); Viola and Jones (2001); Felzenszwalb et al. (2010), the focus is on preserving established levels of accuracy while increasing speed.

3 Structured Prediction Cascades (SPC)

Given an input space \mathcal{X} , output space \mathcal{Y} , and a training set $\{(x^1, y^1), \dots, (x^n, y^n)\}$ of n samples from a joint distribution $D(X, Y)$, the standard supervised learning task is to learn a hypothesis $h : \mathcal{X} \mapsto \mathcal{Y}$ that minimizes the expected loss $\mathbb{E}_D [\mathcal{L}(h(X), Y)]$ for some non-negative loss function $\mathcal{L} : \mathcal{Y} \times \mathcal{Y} \rightarrow \mathbb{R}^+$. In *structured prediction problems*, Y is a ℓ -vector of variables and $\mathcal{Y} = \mathcal{Y}_1 \times \dots \times \mathcal{Y}_\ell$, and $\mathcal{Y}_i = \{1, \dots, K\}$. In many settings, the number of random variables, ℓ , differs depending on input X , but for simplicity of notation, we assume a fixed ℓ here. Note that for the rest of this paper, we will use capital letters X and Y to denote random variables drawn from $D(X, Y)$ and lower-case letters x and y to denote specific values of X and Y . We use subscripts to index elements of y , where y_i is the i th component of y .

The linear hypothesis class we consider is

$$h(x) = \operatorname{argmax}_{y \in \mathcal{Y}} \theta^\top \mathbf{f}(x, y), \quad (1)$$

where the scoring function is the inner product of a vector of parameters $\theta \in \mathbb{R}^d$ and a feature function $\mathbf{f} : \mathcal{X} \times \mathcal{Y} \mapsto \mathbb{R}^d$ mapping (x, y) pairs to a set of features. We further make the standard assumption that \mathbf{f} decomposes over a set of cliques \mathcal{C} over output variables, so that

$$\theta^\top \mathbf{f}(x, y) = \sum_{c \in \mathcal{C}} \theta^\top \mathbf{f}_c(x, y_c). \quad (2)$$

We use the notation y_c to denote the subset of variables involved in clique c , $y_c \triangleq \{y_i \mid i \in c\}$. Similarly, we use $\mathcal{Y}_c \triangleq \mathcal{Y}_{i_1} \times \dots \times \mathcal{Y}_{i_{|c|}}$ where $c = \{i_1, \dots, i_{|c|}\}$, to refer to the set of all assignments to y_c . By considering different cliques over X and Y , \mathbf{f} can represent arbitrary interactions between the components of x and y . Computing the argmax in $h(x)$ is tractable for low-treewidth (hyper)graphs but is NP-hard in general, and approximate inference is typically used when graphs are not low-treewidth. We will abbreviate $\theta^\top \mathbf{f}(x, y)$ as $\theta(x, y)$ below, and similarly $\theta^\top \mathbf{f}_c(x, y)$ as $\theta(x, y_c)$.

In this section, we introduce the framework of Structured Prediction Cascades (SPC) to handle problems for which the inference problem in Eq. 1 is prohibitively expensive. For example, in a 5-th order linear chain model for handwriting recognition or part-of-speech tagging, K is about 50 characters or parts-of-speech, and exact inference is on the order $50^6 \approx 15$ billion times the length the sequence. In tree-structured models we have used for human pose estimation (Sapp et al., 2010b), typical K for each part includes image location and orientation and is on the order of 250,000, so computing K^2 pairwise features is prohibitive. Rather than learning a single monolithic model, a *structured prediction cascade* is a coarse-to-fine sequence of increasingly complex models $\theta^0, \dots, \theta^T$ with corresponding features $\mathbf{f}^0, \dots, \mathbf{f}^T$. For example, inference complexity scales exponentially with Markov order in sequence models, and quadratically with spatial/angular resolution in pose models. The goal of each model is to filter out a large subset of possible values for y without eliminating the

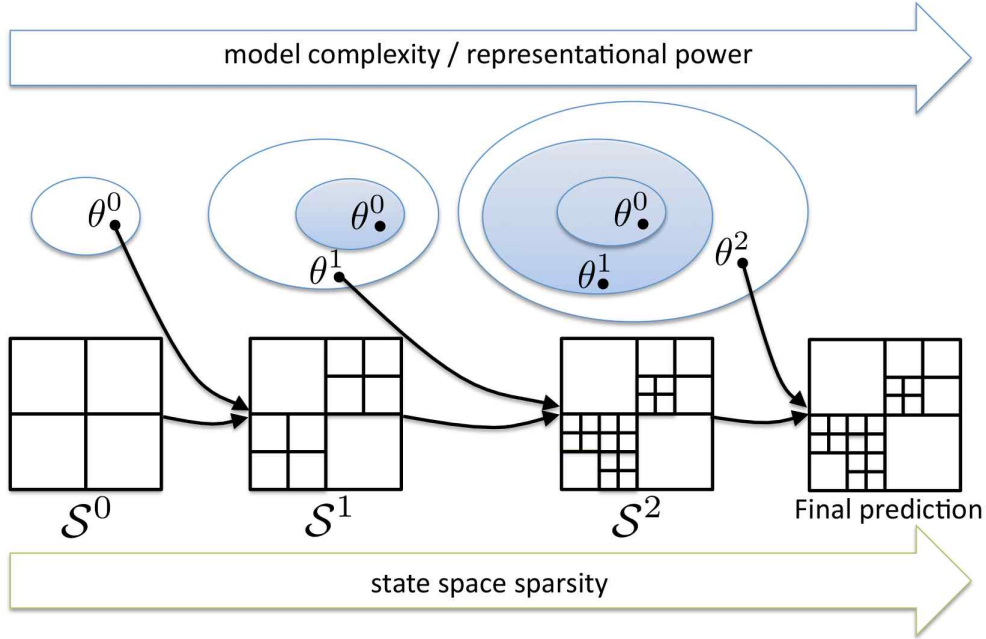


Figure 1: A high-level overview of the SPC inference framework. As the cascade progresses, the representational power of the models increases, yet tractability is maintained by sufficient filtering of the state space.

correct one, so that the next level only has to consider a much reduced state-space. The filtering process is feed-forward, and each stage runs inference to compute *max-marginals* which are used to eliminate low-scoring node or clique assignments.

In summary, a high-level overview of the SPC inference framework is as follows. Below, \mathcal{S}^i denotes a sparse (filtered) version of the output space \mathcal{Y} :

- Given an input x , initialize the cascade with $\mathcal{S}^0 = \mathcal{Y}$.
- Repeat for each level $i = 0, \dots, T - 1$ of the cascade:
 - Run sparse inference over \mathcal{S}^i using model $\theta^i(x, y')$ and eliminate a subset of low-scoring outputs.
 - Output \mathcal{S}^{i+1} for the next model.
- Predict using the final level: $y = \operatorname{argmax}_{y' \in \mathcal{S}^T} \theta^T(x, y')$.

The process is illustrated in Figure 1. See Figure 2 for a concrete example of the output of a the first two stages of a cascade for handwriting recognition (Figure 2) and human pose estimation (Figure 8). We will discuss how to represent and choose \mathcal{S}^i in the next section. The key challenge is that \mathcal{S}^i are exponential in the number of output variables, which rules out explicit representations. The representation we propose is implicit and concise. It is also tightly integrated with parameter estimation algorithm for θ^i that optimizes the overall accuracy and efficiency of the cascade.

3.1 Cascaded inference with max-marginals

In order to filter low-scoring outputs, we use *max-marginals*, for reasons that we detail below. For any value of y_c , we define the max-marginal $\theta^*(x, y_c)$ to be the maximum score of any output y

Symbol	Meaning
\mathcal{X}, X, x	input space, variable and value
\mathcal{Y}, Y, y	output space, variables and value
\mathcal{C}, c, y_c	set of cliques, individual clique, clique assignment
$\mathbf{f}(x, y)$	features of input/output pair
$\mathbf{f}_c(x, y_c)$	features of a clique assignment
$\theta(x, y) \triangleq \theta^\top \mathbf{f}(x, y)$	score of input/output pair
$\theta(x, y_c) \triangleq \theta^\top \mathbf{f}_c(x, y_c)$	score of a clique assignment
$\theta^*(x, y_c) \triangleq \max_{y': y'_c = y_c} \theta(x, y')$	max-marginal of a clique assignment y_c
$y^*(x, y_c; \theta) \triangleq \operatorname{argmax}_{y': y'_c = y_c} \theta(x, y')$	best scoring output consistent with clique assignment y_c

Table 1: Summary of key notation.

that is consistent with the assignment y_c :

$$\theta^*(x, y_c) \triangleq \max_{y': y'_c = y_c} \theta(x, y'). \quad (3)$$

Max-marginals can be computed exactly and efficiently for any clique c in low-treewidth graphs, although the computational cost is exponential in $|c|$ (the number of variables in the clique) when the state-space is not filtered. Note that max-marginals can be computed over *any* clique c , not just the cliques used in the feature function \mathbf{f} ; for example, in Section 6.2, we compute max-marginals over single variables (i.e., $y_c = y_j$ when performing human pose estimation (Figure 8), but at increasingly higher resolutions. On the other hand, in Section 6.1 we compute max-marginals over increasingly large cliques for sequence models (e.g. bigram, trigrams, and quadgrams).

Exact computation of max-marginals for a clique c requires the same amount of time to run as standard exact MAP inference. This process is visualized in Figure 3: once forward and backward max-sum messages have been computed for MAP inference, the max-marginal for a given value y_c is simply the sum of the score $\theta(x, y_c)$ plus the incoming messages to the variables in c . Note that in practice, both stages of computation become faster as the output space becomes increasingly sparse as the input proceeds through the cascade. This algorithm can also compute the maximizing assignment for each y_c ,

$$y^*(x, y_c; \theta) \triangleq \operatorname{argmax}_{y': y'_c = y_c} \theta(x, y'). \quad (4)$$

We call $y^*(x, y_c; \theta)$ the *argmax-marginal* or *witness* for y_c (it might not be unique, so we break ties in an arbitrary but deterministic way).

Once max-marginals have been computed, we filter the output space by discarding any clique assignments y_c for which $\theta^*(x, y_j) \leq t$ for a threshold t (Figure 4). This filtering rule has two desirable properties for the cascade that follow immediately from the definition of max-marginals:

Lemma 1 (Safe Filtering). *If $\theta(x, y) > t$, then $\forall c \ \theta^*(x, y_c) > t$.*

Lemma 2 (Safe Lattices). *If $\max_{y'} \theta(x, y') > t$, then $\exists y \ \forall c \ \theta^*(x, y_c) > t$.*

By Lemma 1, ensuring that the score of the true label $\theta(x, y)$ is greater than the threshold is sufficient (although not necessary) to guarantee that no marginal assignment y_c consistent with the true global assignment y will be filtered. This condition will allow us to define a max-marginal based loss function that we propose to optimize in Section 4 and will analyze in Section 5. Lemma 2 follows from Lemma 1, which states that so long as the threshold is less than the maximizing score, there always exists a global assignment y with no pruned cliques (i.e., a valid assignment

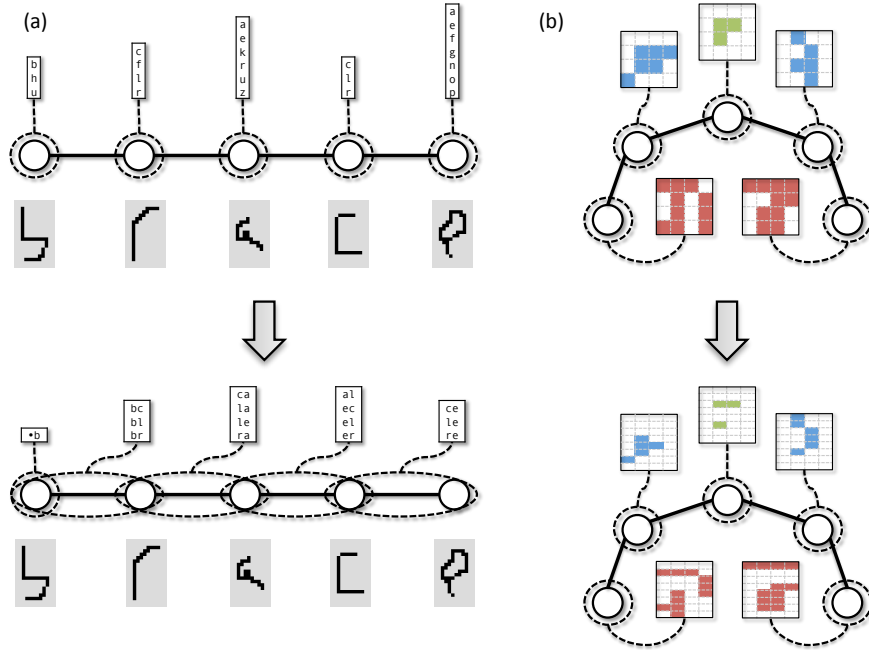


Figure 2: Sample output from the first two layers of a cascade. Circles represent output variables, and the dashed lines indicate cliques that are being filtered at a given level of the cascade, with the attached tables representing the sparse state space. The solid lines indicate the graph used for inference and features. **(a)** Output from a handwriting recognition cascade (Section 6.1) of increasing Markov order. The first level outputs a sparse set of possible letters for each image. The second level takes as input the sparse set of letters, and further refines this to a very sparse set of *bigrams* at each position. **(b)** Output from a coarse-to-fine human pose cascade (Section 6.2). The colored areas indicate valid 2D locations for each joint. Unlike the sequence cascade (a), the cliques stay the same from one layer to another. Instead, the resolution of the state space doubles with each additional layer.

always exists after pruning). Thus, Lemma 2 guarantees that $|\mathcal{S}^{i+1}| \geq 1$ in the SPC algorithm introduced above, and therefore the cascade will always produce a valid output. Note that neither property generally holds for standard sum-product marginals $p(y_c|x)$ of a log-linear CRF (where $p(y|x) \propto e^{\theta(x,y)}$), which motivates our use of max-marginals.

The next component of the inference procedure is choosing a threshold t for a given input x (Figure 4). Note that the threshold cannot be defined as a single global value but should instead depend strongly on the input x and $\theta(x, \cdot)$ since scores are on different scales for different x . We also have the constraint that computing a threshold function must be fast enough such that sequentially computing scores and thresholds for multiple models in the cascade does not adversely effect the efficiency of the whole procedure. One might choose a quantile function to consistently eliminate a desired proportion of the max-marginals for each example. However, quantile functions are discontinuous in θ function, and we instead approximate a quantile threshold with a threshold function that is continuous and convex in θ . We call this the *max-mean-max* threshold function (Figure 4), and define it as a convex combination of the maximum score and the mean of the max-marginals:

$$\tau(x; \theta, \alpha) = \alpha \max_y \theta(x, y) + (1 - \alpha) \frac{1}{\sum_{c \in \mathcal{C}} |\mathcal{Y}_c|} \sum_{c \in \mathcal{C}} \sum_{y_c \in \mathcal{Y}_c} \theta^*(x, y_c). \quad (5)$$

Choosing a threshold using (5) is therefore equivalent to picking a $\alpha \in [0, 1)$. Note that $\tau(x; \theta, \alpha)$ is

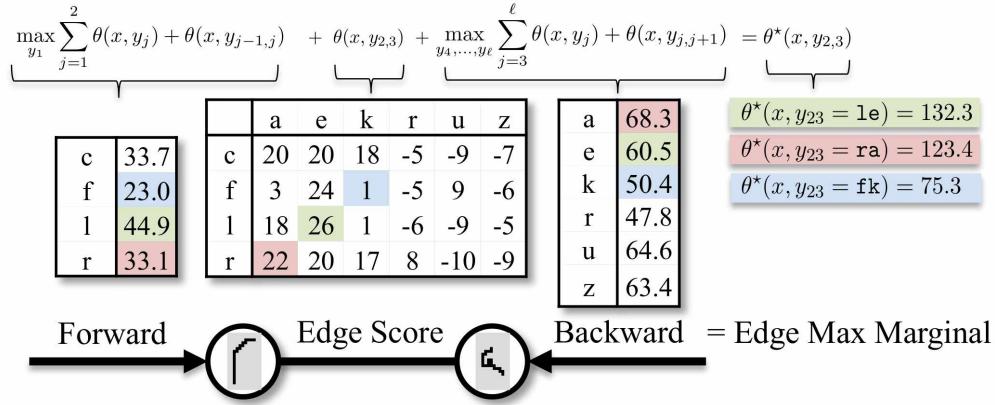


Figure 3: Computing max-marginals over bigrams via message passing. The input is the same as in Figure 2. Once forward and backward messages have been computed, the max-marginal is simply the sum of incoming messages and the score of the clique over bigrams.

a convex function of θ (in fact, piece-wise linear), which combined with Lemma 1 will be important for learning the filtering models and analyzing their generalization. In our experiments, we found that the distribution of max-marginals was well centered around the mean, so that choosing $\alpha \approx 0$ resulted in $\approx 50\%$ of max-marginals being eliminated on average. As α approaches 1, the number of max-marginals eliminated rapidly approaches 100%.²

In summary, the inner loop of the SPC algorithm can be detailed as follows. The sparse output space \mathcal{S}^i is a list of valid assignments y_c for each clique c in the model \mathbf{f}_i (e.g., Figure 2):

$$\mathcal{S}^i = \{\mathcal{Y}_c \mid \forall c \in \mathcal{C}\} \quad (\text{list of valid clique values for all cliques}) \quad (6)$$

Next, sparse max-sum message passing is used to compute max-marginals $\theta^*(x, y_c)$ (3) for each value $y_c \in \mathcal{Y}_c$ of each clique c of interest. Finally, for a given α , a threshold is computed and low-scoring values of $\theta^*(x, y_c)$ are eliminated. Depending on the model in the next layer of the cascade, further transformation of the states may be necessary: For example, in the coarse-to-fine pose cascade (Section 6.2), valid 2-D locations for each limb are halved either vertically or horizontally to produce finer-resolution states for the next model (Figure 2b).

3.2 Cascaded Inference in Loopy Graphs

Thus far, we have assumed that (sparse) inference is feasible, so that max marginals can be computed. In this section, we describe how to apply SPC when exact max-sum message passing is computationally infeasible due to loops in the graph structure of the model. In order to simplify the presentation in this section, we will assume that the structured cascade under consideration operates in a “node-centric” coarse-to-fine manner as follows: For each variable y_j in the model, each level of the cascade filters a current set of possible states \mathcal{Y}_j , and any surviving states are passed forward to the next level of the cascade by substituting each state with its set of descendents in a hierarchy. For example, such hierarchies arise in pose estimation (Section 6.2) by discretizing the articulation of joints at multiple resolutions, or in image segmentation due to the semantic relationship between class labels (e.g., “grass” and “tree” can be grouped as “plants,” “horse” and “cow” can be grouped as “animal.”) Thus, in the pose estimation problem, surviving states are

²We use cross-validation to determine the optimal α in our experiments (see Section 6).

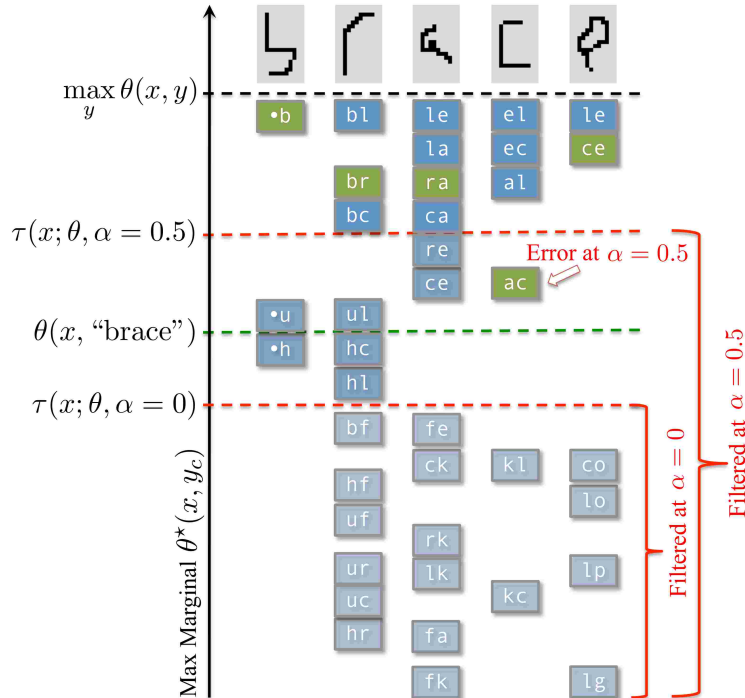


Figure 4: Thresholding bigrams using max-marginals. The input is the same as in Figure 2. The sparse set of unfiltered bigrams is shown at each position according to the max-marginal score. The bigrams corresponding to the correct label sequence, **brace**, are highlighted in green. The green dashed line indicates the score of the correct label sequence. Note that the max-marginals of the correct sequence are at least the score of the correct sequence. The black dashed line indicates the maximum score of any sequence, which is the maximum filtering threshold. The largest max-marginal values are all exactly equal to this score. The red dashed lines indicate two candidate filtering thresholds $\tau(x; \theta, \alpha) = 0$ and $\tau(x; \theta, \alpha) = 0.5$ and corresponding sets of filtered bigrams are highlighted. Note that a filtering error occurs at the more aggressive level of $\alpha = 0.5$.

subdivided into multiple finer-resolution states; in the image segmentation problem, broader object classes are split into their constituent classes for the next level.

The key idea of this section is that we decompose the loopy model into a collection of equivalent tractable sub-models for which inference is tractable. What distinguishes this approach from other decomposition based methods (e.g., Komodakis et al. (2007); Bertsekas (1999)) is that, because the cascade’s objective is filtering and not decoding, our approach does not require enforcing the constraint that the sub-models agree on which output has maximum score. In preliminary work (Weiss et al., 2010), this approach was called *structured ensemble cascades*, here we simply refer to it as Ensemble-SPC.

Given a loopy (intractable) graphical model, it is always possible to express the score of a given output $\theta(x, y)$ as the sum of P scores $\theta_p(x, y)$ under sub-models that collectively cover every edge in the loopy model: $\theta(x, y) = \sum_p \theta_p(x, y)$ (Figure 5). However, it is *not* the case that optimizing each individual sub-model separately will yield the single globally optimum solution. Instead, care must be taken to enforce agreement between sub-models. For example, in the method of dual decomposition (Komodakis et al., 2007), it is possible to solve a relaxed MAP problem in the (intractable) full model by running inference in the (tractable) sub-models under the constraint that *all sub-models agree on the argmax solution*. Enforcing this constraint requires iteratively

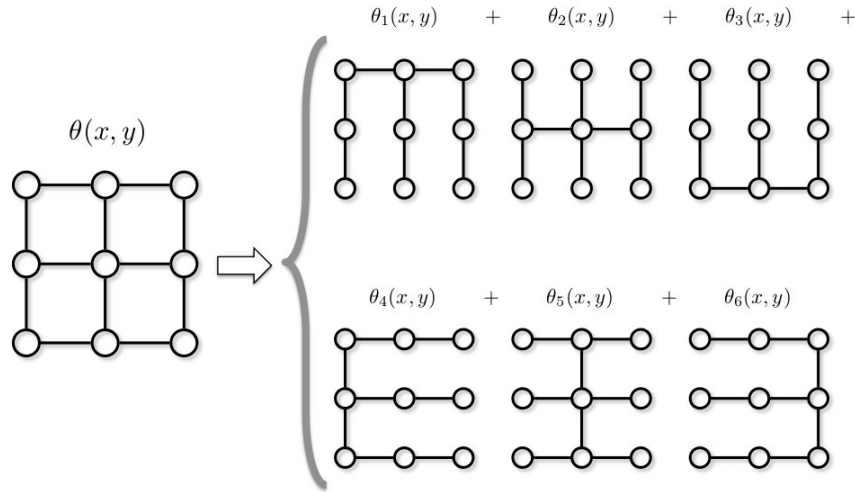


Figure 5: Example decomposition of a 3×3 fully connected grid into all six constituent “comb” trees. In general, a $n \times n$ grid yields $2n$ such trees.

re-weighting unary potentials of the sub-models and repeatedly re-running inference until each sub-model converges to the same argmax solution.

However, for the purposes of SPC, we are only interested in computing the max-marginals $\theta^*(x, y_j)$. In other words, we are only interested in knowing whether or not a configuration y consistent with y_j that scores highly in each sub-model $\theta_p(x, y)$ *exists*. We show in the remainder of this section that the requirement that a *single* y consistent with y_j optimizes the score of each submodel (i.e, that all sub-models *agree*) is not necessary for the purposes of filtering. Thus, because we do not have to enforce agreement between sub-models, we can apply SPC to intractable (loopy) models, but pay only a linear (factor of P) increase in inference time over the tractable sub-models.

Formally, we define a single level of the Ensemble-SPC as a set of P models such that $\theta(x, y) = \sum_p \theta_p(x, y)$. We let $\theta_p^*(x, y_c)$, $\theta_p^*(x)$ and $\tau(x; \theta_p, \alpha)$ denote the max-marginals, max score, and threshold of the p 'th model, respectively. Recall that the *argmax-marginal* or *witness* $y^*(x, y_j; \theta_p)$ is defined as the maximizing complete assignment of the corresponding max-marginal $\theta_p^*(x, y_j)$. Then we have that

$$\theta^*(x, y_j) = \sum_p \theta_p^*(x, y_j) \quad (\text{with agreement: } y = y^*(x, y_j; \theta_p), \forall p) \quad (7)$$

$$\theta^*(x, y_j) \leq \sum_p \theta_p^*(x, y_j) \quad (\text{in general}) \quad (8)$$

Note that if we do not require the sub-models to agree, then $\theta^*(x, y_j)$ is strictly less than $\sum_p \theta_p^*(x, y_j)$. Nonetheless, as we show next, the approximation $\theta^*(x, y_j) \approx \sum_p \theta_p^*(x, y_j)$ is still useful and sufficient for filtering in a structured cascade.

We now show that if a given label y has a high score in the full model, it must also have a large ensemble max-marginal score, even if the sub-models do not agree on the argmax. This extends Lemma 1 for the ensemble case, as follows:

Lemma 3 (Joint Safe Filtering). *If $\sum_p \theta_p(x, y) > t$, then $\sum_p \theta_p^*(x, y_j) > t$ for all j .*

Proof. In English, this lemma states that if the global score is above a given threshold, then the sum of sub-model max-marginals is also above threshold (with no agreement constraint). The

proof is straightforward. For any y_j consistent with y , we have $\theta_p^*(x, y_j) \geq \theta_p(x, y)$. Therefore $\sum_p \theta_p^*(x, y_j) \geq \sum_p \theta_p(x, y) > t$. \square

Therefore, we see that an agreement constraint is not necessary in order to filter safely: if we ensure that the combined score $\sum_p \theta_p(x, y)$ of the true label y is above threshold, then we can filter without making a mistake if we compute max-marginals by running inference separately for each sub-model. However, there is still potentially a price to pay for disagreement. If the sub-models do not agree, *and* the truth is not above threshold, then the threshold may filter *all* of the states for a given variable y_j and therefore “break” the cascade. This results from the fact that without agreement, there is no single argmax output y^* that is always above threshold for any α ; therefore, we do not have an equivalent to Lemma 2 for the ensemble case. However, we note that in our experiments (Section 6.3), we never experienced such breakdown of the cascades.

4 Learning Structured Prediction Cascades

When learning a cascade, we have two competing objectives that we must trade off:

- **Accuracy:** Minimize the number of errors incurred by each level of the cascade to ensure an accurate inference process in subsequent models.
- **Efficiency:** Maximize the number of filtered max-marginals at each level in the cascade to ensure an efficient inference process in subsequent models.

Given a training set, we can measure the accuracy and efficiency of our cascade, but what is unknown is the performance of the cascade on test data. In section 5, we provide a guarantee that our estimates of accuracy and efficiency will be reasonably close to the true performance measures with high probability. This suggests that optimizing parameters to achieve a desired trade-off on training data is a good idea.

We begin by quantifying accuracy and efficiency in terms of max-marginals, as used by SPC. We define the *filtering loss* \mathcal{L}_f to be a 0-1 loss indicating a mistakenly eliminated correct assignment. As discussed in the previous section, Lemma 1 states that an error can only occur if $\theta(x, y) \leq \tau(x; \theta, \alpha)$. We also define the *efficiency loss* \mathcal{L}_e to simply be the proportion of unfiltered clique assignments.

Definition 1 (Filtering loss). *A filtering error occurs when a max-marginal of a clique assignment of the correct output y is pruned. We define filtering loss as*

$$\mathcal{L}_f(x, y; \theta, \alpha) = \mathbf{1}[\theta(x, y) \leq \tau(x; \theta, \alpha)]. \quad (9)$$

Definition 2 (Efficiency loss). *The efficiency loss is the proportion of unpruned clique assignments:*

$$\mathcal{L}_e(x, y; \theta, \alpha) = \frac{1}{\sum_{c \in \mathcal{C}} |\mathcal{Y}_c|} \sum_{c \in \mathcal{C}, y_c \in \mathcal{Y}_c} \mathbf{1}[\theta^*(x, y_c) > \tau(x; \theta, \alpha)]. \quad (10)$$

We now turn to the problem of learning parameters θ and tuning of the threshold parameter α from training data. We have two competing objectives, accuracy (\mathcal{L}_f) and efficiency (\mathcal{L}_e), that we must trade off. Note that we can trivially minimize either of these at the expense of maximizing the other. If we set (θ, α) to achieve a minimal threshold such that no assignments are ever filtered, then $\mathcal{L}_f = 0$ and $\mathcal{L}_e = 1$. Alternatively, if we choose a threshold to filter every assignment, then $\mathcal{L}_f = 1$ while $\mathcal{L}_e = 0$. To learn a cascade of practical value, we can minimize one loss while constraining the other below a fixed level ϵ . Since the ultimate goal of the cascade is accurate classification, we

Algorithm 1 Forward Batch Learning of Structured Prediction Cascades.

Input: Data $\{(x^i, y^i)\}_1^n$, structured feature generators $\mathbf{f}^0, \dots, \mathbf{f}^T$ and parameters $\alpha^0, \dots, \alpha^{T-1}$.

Output: Cascade parameters $\theta^0, \dots, \theta^T$.

Initialize $\mathcal{S}^0(x^i) = \mathcal{Y}(x^i)$ for each example.

for $t = 0$ **to** $T - 1$ **do**

- Optimize (12) with sparse inference over the valid set \mathcal{S}^t to find θ^t .
- Generate $\mathcal{S}^{t+1}(x^i)$ from $\mathcal{S}^t(x^i)$ by filtering low-scoring clique assignments y_c where

$$\theta^{t*}(x^i, y_c) \leq \tau(x^i; \theta^t, \alpha^t)$$

end for

- Learn θ^T using structured predictor over sparse state spaces $\mathcal{S}^T(x^i)$.
-

focus on the problem of minimizing efficiency loss while constraining the filtering loss to be below a desired tolerance.

We express the cascade learning objective for a *single level* of the cascade as a joint optimization over θ and α :

$$\min_{\theta, \alpha} \mathbb{E}_{X, Y} [\mathcal{L}_e(X, Y; \theta, \alpha)] \text{ s.t. } \mathbb{E}_{X, Y} [\mathcal{L}_f(X, Y; \theta, \alpha)] \leq \epsilon. \quad (11)$$

We solve this problem with for a single level of the cascade as follows. First, we define a convex upper-bound (12) on the filter error \mathcal{L}_f , making the problem of minimizing \mathcal{L}_f convex in θ (given α). We learn θ to minimize filter error for several settings of α (thus controlling filtering efficiency). Given several possible values for θ , we optimize the objective (11) over α directly, using estimates of \mathcal{L}_f and \mathcal{L}_e computed on a held-out development set, and choose the best θ . Note that in Section 5, we present a theorem bounding the deviation of our estimates of the efficiency and filtering loss from the expectation of these losses.

For the first step of learning a single level of the cascade, we learn the parameters θ for a fixed α using the following convex margin optimization problem:

$$SPC : \quad \min_{\theta} \quad \frac{\lambda}{2} \|\theta\|^2 + \frac{1}{n} \sum_i H(x^i, y^i; \theta, \alpha), \quad (12)$$

where H is a convex upper bound on the filter loss \mathcal{L}_f ,

$$H(x^i, y^i; \theta, \alpha) = \max\{0, \ell + \tau(x^i; \theta, \alpha) - \theta(x^i, y^i)\}.$$

The upper-bound H is a hinge loss measuring the margin between the filter threshold $\tau(x^i; \theta, \alpha)$ and the score of the truth $\theta^\top \mathbf{f}(x^i, y^i)$; the loss is zero if the truth scores above the threshold by margin ℓ (in practice, the length ℓ can vary by example). We solve (12) using stochastic sub-gradient descent. Given a sample (x, y) , we apply the following update if $H(\theta, x, y)$ (i.e., the sub-gradient) is non-zero:

$$\theta' \leftarrow (1 - \eta\lambda)\theta + \eta \mathbf{f}(x, y) - \eta \alpha \mathbf{f}(x, y^*) - \eta(1 - \alpha) \frac{1}{\sum_c |\mathcal{Y}_c|} \sum_{c \in \mathcal{L}, y_c \in \mathcal{Y}} \mathbf{f}(x, y^*(x, y_c; \theta)). \quad (13)$$

Above, η is a learning rate parameter. The key distinguishing feature of this update compared to the structured perceptron update is that it subtracts features included in all max-marginal assignments $y^*(x, y_c; \theta)$.

Note that because (12) is λ -strongly convex, we can choose $\eta_t = 1/(\lambda t)$ and add a projection step to keep θ in a fixed norm-ball. The update then corresponds to the Pegasos update with convergence guarantees of $\tilde{O}(1/\epsilon)$ iterations for ϵ -accurate solutions (Shalev-Shwartz et al., 2007).

An overview of the entire learning process for the whole cascade is given in Algorithm 1. Levels of the cascade are learned incrementally using the output of the previous level of the cascade as input. Note that Algorithm 1 trades memory efficiency for time efficiency by storing the sparse data structures \mathcal{S}^t for each example. A more memory-efficient (but less time efficient) algorithm would instead run all previous layers of the cascade for each example during sub-gradient descent optimization of (12).

Finally, in our implementation, we can sometimes achieve better results by further tuning the threshold parameters α^t using a development set. We first learn θ^t using some fixed α^t as before. However, we then choose an improved $\bar{\alpha}^t$ by maximizing efficiency subject to the constraint that filter loss on the development set is less than a *tolerance* ϵ_t :

$$\bar{\alpha}^t \leftarrow \operatorname{argmin}_{0 \leq \alpha' < 1} \sum_{i=1}^n \mathcal{L}_e(x^i, y^i; \theta^t, \alpha') \quad \text{s.t.} \quad \frac{1}{n} \sum_{i=1}^n \mathcal{L}_f(x^i, y^i; \theta^t, \alpha') \leq \epsilon_t.$$

Furthermore, we can repeat this tuning process for several different starting values of α^t and pick the $(\theta^t, \bar{\alpha}^t)$ pair with the optimal trade-off, to further improve performance. In practice, we find that this procedure can substantially improve the efficiency of the cascade while keeping accuracy within range of the given tolerance.

It is straightforward to adapt Algorithm 1 for the Ensemble-SPC case. As in the previous section, we first define the natural loss function for sums of max-marginals, as suggested by Lemma 3. We define the *joint filtering loss* as follows,

Definition 3 (Joint Filtering Loss).

$$\mathcal{L}_{\text{joint}}(x, y; \theta, \alpha) = \mathbf{1} \left[\sum_p \theta_p(x, y) \leq \sum_p \tau(x; \theta_p, \alpha) \right]. \quad (14)$$

We now discuss how to minimize the *joint* filter loss (14) given a dataset. We rephrase the SPC optimization problem (12) using the ensemble max-marginals to form the ensemble cascade margin problem,

$$\min_{\theta_1, \dots, \theta_P, \xi \geq 0} \frac{\lambda}{2} \sum_p \|\theta_p\|^2 + \frac{1}{n} \sum_i \xi^i \quad \text{s.t.} \quad \sum_p \theta_p(x^i, y^i) \geq \sum_p \tau(x^i; \theta_p, \alpha) + \ell^i - \xi^i. \quad (15)$$

Seeing that the constraints can be ordered to show $\xi^i \leq \sum_p \tau(x^i; \theta_p, \alpha) - \sum_p \theta_p(x^i, y^i) + \ell^i$, we can form an equivalent unconstrained minimization problem,

$$\min_{\theta_1, \dots, \theta_P} \frac{\lambda}{2} \sum_p \|\theta_p\|^2 + \frac{1}{n} \sum_i \left[\sum_p \tau(x^i; \theta_p, \alpha) - \sum_p \theta_p(x^i, y^i) + \ell^i \right]_+, \quad (16)$$

where $[z]_+ = \max\{z, 0\}$. Finally, we take the subgradient of the objective in (16) with respect to each parameter θ_p . This yields the following update rule for the p 'th model:

$$\theta_p \leftarrow (1 - \lambda)\theta_p + \begin{cases} 0 & \text{if } \sum_p \theta_p(x^i, y^i) \geq \sum_p \tau(x^i; \theta_p, \alpha) + \ell^i, \\ \nabla \theta_p(x^i, y^i) - \nabla \tau(x^i; \theta_p, \alpha) & \text{otherwise.} \end{cases} \quad (17)$$

This update is identical to the original SPC update with the exception that we update each model individually only when the ensemble has made a mistake *jointly*. Thus, learning to filter with the ensemble requires only P times as many resources as learning to filter with any of the models individually. We simply replace the optimization over (12) step in Algorithm 1 with an optimization over (16).

5 Generalization Analysis

We now present generalization bounds on the filtering and efficiency loss functions for a single level of a cascade. To achieve bounds on the entire cascade, these can be combined provided that a fresh sample is used for each level. To prove the following bounds, we make use of Gaussian complexity results from Bartlett and Mendelson (2002), which requires vectorizing scoring and loss functions in a novel structured manner (details in Appendix A). The main theorem in this section depends on Lipschitz dominating cost functions \mathcal{L}_f^γ and \mathcal{L}_e^γ that upper bound \mathcal{L}_f and \mathcal{L}_e . Note that as $\gamma \rightarrow 0$, we recover \mathcal{L}_f and \mathcal{L}_e .

Definition 4 (Margin-augmented losses). *We define margin-augmented filtering and efficiency losses using the usual γ -margin function:*

$$r_\gamma(z) = \begin{cases} 1 & \text{if } z < 0 \\ 1 - z/\gamma & \text{if } 0 \leq z \leq \gamma \\ 0 & \text{if } z > \gamma. \end{cases} \quad (18)$$

$$\mathcal{L}_f^\gamma(x, y; \theta, \alpha) = r_\gamma(\theta(x, y) - \tau(x; \theta, \alpha)) \quad (19)$$

$$\mathcal{L}_e^\gamma(x, y; \theta, \alpha) = \frac{1}{\sum_{c \in \mathcal{C}} |\mathcal{Y}_c|} \sum_{c \in \mathcal{C}, y_c \in \mathcal{Y}_c} r_\gamma(\tau(x; \theta, \alpha) - \theta^*(x, y_c)). \quad (20)$$

Theorem 1. *Fix $\alpha \in [0, 1]$ and let Θ be the class of all scoring functions θ with $\|\theta\|_2 \leq B$, let $|\mathcal{C}|$ be the total number of cliques, $m = \sum_{c \in \mathcal{C}} |\mathcal{Y}_c|$ be the total number of clique assignments, $\|\mathbf{f}_c(x, y_c)\|_2 \leq 1$ for all $x \in \mathcal{X}, c \in \mathcal{C}$ and $y_c \in \mathcal{Y}_c$. Then there exists a constant c such that for any integer n and any $0 < \delta < 1$ with probability $1 - \delta$ over samples of size n , every $\theta \in \Theta$ satisfies:*

$$\mathbb{E}[\mathcal{L}_f(X, Y; \theta, \alpha)] \leq \hat{\mathbb{E}}[\mathcal{L}_f^\gamma(X, Y; \theta, \alpha)] + \frac{cmB\sqrt{|\mathcal{C}|}}{\gamma\sqrt{n}} + \sqrt{\frac{8\ln(2/\delta)}{n}}, \quad (21)$$

$$\mathbb{E}[\mathcal{L}_e(X, Y; \theta, \alpha)] \leq \hat{\mathbb{E}}[\mathcal{L}_e^\gamma(X, Y; \theta, \alpha)] + \frac{cmB\sqrt{|\mathcal{C}|}}{\gamma\sqrt{n}} + \sqrt{\frac{8\ln(2/\delta)}{n}}, \quad (22)$$

where $\hat{\mathbb{E}}$ is the empirical expectation with respect to the sample.

Theorem 1 provides theoretical justification for the definitions of the loss functions \mathcal{L}_e and \mathcal{L}_f and the structured cascade objective; if we observe a highly accurate and efficient filtering model (θ, α) on a finite sample of training data, it is likely that the performance of the model on unseen test data will not be too much worse as n gets large. Theorem 1 is the first theoretical guarantee on the generalization of *accuracy* and *efficiency* of a structured filtering model.

We now turn to ensemble setting and define an appropriate margin-augmented loss:

Definition 5 (Ensemble margin-augmented loss).

$$\mathcal{L}_{joint}^\gamma(x, y; \theta, \alpha) = r_\gamma\left(\sum_p \theta_p(x, y) - \tau(x; \theta_p, \alpha)\right) \quad (23)$$

Theorem 2. Fix $\alpha \in [0, 1]$ and let $\|\theta_p\|_2 \leq B/P$ for all p , and $\|\mathbf{f}_c(x, y_c)\|_2 \leq 1$ for all x and y_c . Then there exists a constant c such that for any integer n and any $0 < \delta < 1$ with probability $1 - \delta$ over samples of size n , every $\theta = \{\theta_1, \dots, \theta_P\}$ satisfies:

$$\mathbb{E}[\mathcal{L}_{\text{joint}}(X, Y; \theta, \alpha)] \leq \hat{\mathbb{E}}[\mathcal{L}_{\text{joint}}^\gamma(X, Y; \theta, \alpha)] + \frac{cmBP\sqrt{|\mathcal{C}|}}{\gamma\sqrt{n}} + \sqrt{\frac{8\ln(2/\delta)}{n}}, \quad (24)$$

where $\hat{\mathbb{E}}$ is the empirical expectation with respect to the sample.

The proof of Theorem 2 is given in Appendix A.

6 Applications

In this section, we explore in detail several evaluations of structured prediction cascades. In Section 6.1 we describe a structured prediction cascade for sequential data and apply this model handwriting recognition. In Section 6.2, we describe SPC for articulated human pose estimation from single frame images. Finally, in Section 6.3, we evaluate Ensemble-SPC on a synthetic image segmentation task and the problem of *detection and tracking* articulated poses in video.

6.1 Linear-chain Cascade

In this section, we apply the structured prediction cascades framework to sequence prediction tasks with increasingly high order linear-chain models. The state space of a linear chain model is $\forall i : \mathcal{Y}_i = \{1, \dots, K\}$, where K is the number of possible states. Thus, the size of the state space is K . A d -order linear-chain model has maximal cliques $\{x, y_i, y_{i-1}, \dots, y_{i-d}\}$. Thus, for an order d clique, there are K^d possible clique assignments, although we find that in practice very few high-order clique assignments survive the first few levels of the cascade (see Table 2.)

For a d -order linear-chain model, the score of an output y is given by a combination of unary features and transition features,

$$\theta(x, y) = \sum_{i=1}^{\ell} \theta_0^\top \mathbf{f}_0(x, y_i) + \sum_{i=1}^{\ell} \sum_{j=1}^d \theta_j^\top \mathbf{f}_j(y_i, \dots, y_{i-j}) \quad (25)$$

where θ_0 is a set of parameters for unary features $\mathbf{f}(x, y_i)$ that depend on a single output variable and θ_j is a set of parameters scoring j -order transition features $\mathbf{f}_j(y_i, \dots, y_{i-j})$.

In general, any d -order linear-chain model can be equivalently represented as a bigram (2-order) model with K^{d-1} states. Thus, it is simplest to implement a cascade of sequence models of increasing order as a set of bigram models where the state space is increasing exponentially by a factor of K from one model to the next. Given a list of valid assignments \mathcal{S}^t in a d -order model, we can generate an expanded list of valid assignments \mathcal{S}^{t+1} for a $(d+1)$ -order model by concatenating the valid d -grams with all possible additional states.

6.1.1 Handwriting Recognition

We first evaluated the accuracy of the cascade using the handwriting recognition dataset from Taskar et al. (2003). This dataset consists of 6877 handwritten words, with average length of ~ 8 characters, from 150 human subjects, from the data set collected by Kassel (1995). Each word was segmented into characters, each character was rasterized into an image of 16 by 8 binary pixels. The dataset is divided into 10 folds; we used 9 folds for training and a single withheld for testing

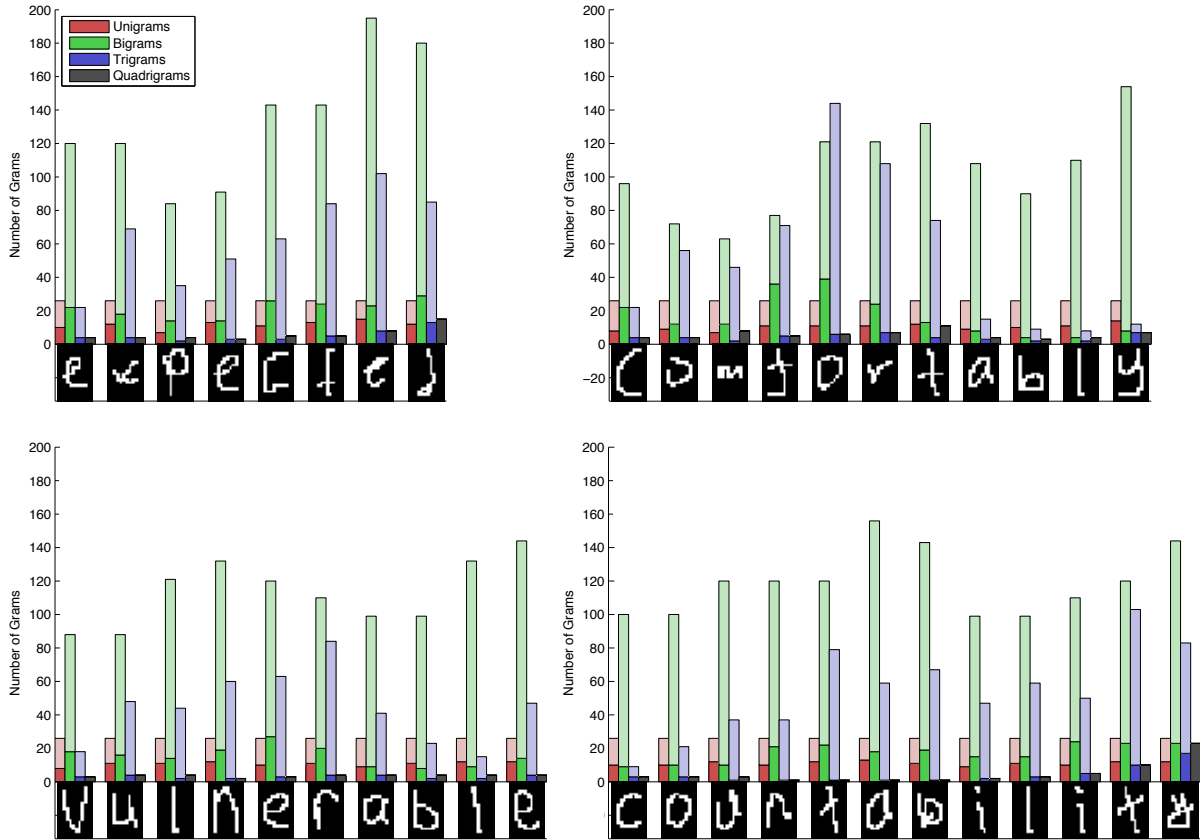


Figure 6: Sparsity of inference during an example sequence cascade. Each panel shows the complexity of inference on a different example from the OCR dataset at each position in the sequence. The total height of each bar represents the size of the valid assignments \mathcal{S}^t , while the shaded portion represents the remaining assignments after thresholding. Although complexity rises as unigrams are expanded into bigrams, filtering with bigrams and trigrams quickly reduces complexity to a few possible assignments at each position.

(note that Taskar et al. (2003) used 9 folds for testing and 1 for training due to computational limitations, so our results are not directly comparable). Results are averaged across all 10 folds.

Our objective was to measure the improvement in predictive accuracy as higher order models were incorporated into the cascade. We trained six cascades, up to a sixth-order (sexagram) linear-chain model. This is significantly higher order than the typical third-order (trigram) models typically used in sequence classification tasks. Note that in practice, the additional accuracy gained by increasing the order of the model might be offset by the additional filtering errors incurred due to lengthening the cascade. Thus, each level of each cascade was tuned to achieve maximum efficiency subject to a maximum error *tolerance* ϵ , whereby α was set such that no more than ϵ filtering error was incurred by each level of the cascade.

Results are summarized in Table 2. We found that using higher order models led to a dramatic gain in accuracy on this dataset, increasing character accuracy from 77.35% to 98.54% and increasing word accuracy from 26.74% to 96.16%. It is interesting to note that the word level accuracy of the sixth-order model is roughly equivalent to the character-level accuracy of the trigram model. Furthermore, using a development set, we found that a stricter tolerance was required to gain accuracy from fifth- and sixth-order models, as reflected in Table 2. Finally, compared to previous

Model Order	1	2	3	4	5	6
Accuracy, Char. (%)	77.35	85.02	96.20	97.21	98.27	98.54
Accuracy, Word (%)	26.74	45.67	88.25	91.35	93.74	96.16
Filter Loss (%)	—	0.50	0.73	1.00	0.75	0.57
Tolerance (%)	1.00	1.00	1.00	1.00	0.50	0.25
Avg. Num n -grams	26.0	127.97	101.84	18.80	82.12	73.36

Table 2: Summary of handwriting recognition results. For each level of the cascade, we computed prediction accuracy (at character and word levels) using a standard voting perceptron algorithm as well as the filtering loss and average number of unfiltered n -grams per position for the SPC on the test set.

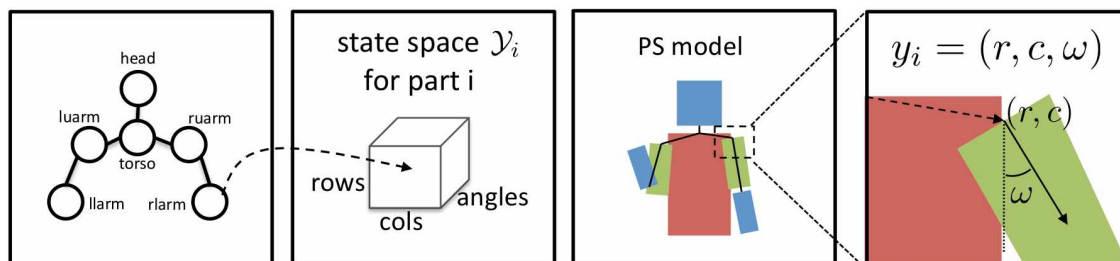


Figure 7: Basic PS model with state y_i for a part Y_i . Left: graphical model representation. Second: state space representation as a tensor. Rightmost two panels: Illustration of state space laid out as a stick figure representation in image coordinates.

approaches on this dataset, our accuracies are much higher; the best previously reported result on this dataset was 90.19% (Daumé et al., 2009).

In fact, the extremely high accuracies of our approach on this dataset highlight the particular features of this data. Due to the high number of subjects used, there are only 55 unique words in the handwriting recognition dataset. In fact, if just the first three letters of each word are given exactly, one can guess the identity of the word with 94.5% accuracy. Given more letters, it is possible to uniquely identify the word with 100% accuracy. However, due to inter-subject variance, previous approaches have not been able approach this theoretical performance. By being able to utilize very high order cliques, SPC overcomes this limitation.

To gain intuition about the inference process of SPC, a detailed picture of the complexity of inference for a few representative examples is presented in Figure 6 for the fourth-order cascade model. This figure also demonstrates the flexibility of the cascade: although a single threshold is chosen, the max marginals around unambiguous portions of the input are eliminated first.

6.2 Pictorial Structure Cascade

Classical pictorial structures (PS) are a class of graphical models where the nodes of the graph represents object parts, and edges between parts encode pairwise geometric relationships. For modeling human pose, the standard PS model is a tree structure with unary potentials (also referred to as appearance terms) for each part and pairwise terms between pairs of physically connected parts. Figure 7 shows a PS model for 6 upper body parts, with lower arms connected to upper arms, and upper arms and head connected to torso. Note that in previous work (Ramanan and Sminchisescu, 2006; Felzenszwalb and Huttenlocher, 2005; Ferrari et al., 2008; Andriluka et al., 2009) (unlike the approach described in this section), the pairwise terms do not depend on data and are hence referred to as a “spatial” or “structural” prior.

The state of part i , denoted as $y_i \in \mathcal{Y}_i$, encodes the joint location of the part in image coordinates

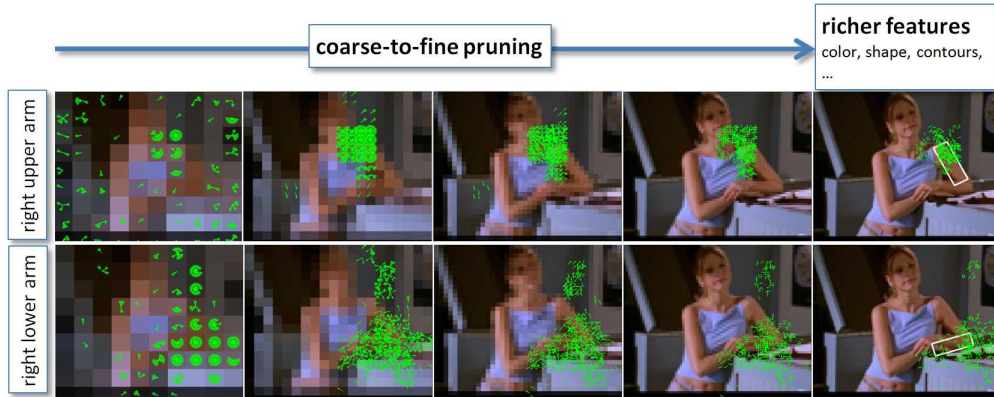


Figure 8: Overview: A coarse-to-fine cascade of pictorial structures filters the pose space so that expressive and computationally expensive features can be used in the final pictorial structure. Shown are 5 levels of the coarse-to-fine cascade for the right upper and lower arm parts. Green vectors represent position and angle of unpruned states, the downsampled images correspond to the dimensions of the respective state space, and the white rectangles represent classification using our final model.

and the direction of the limb as a unit vector: $y_i = [y_{ix} \ y_{iy} \ y_{iu} \ y_{iv}]^T$. The state of the model is the collection of states of ℓ parts: $y = [y_1, \dots, y_\ell]$. The size of the state space for each part, $|\mathcal{Y}_i|$, is the number of possible locations in the image times the number of pre-defined discretized angles. For example, we model the state space of each part in a 80×80 grid for $y_{ix} \times y_{iy}$, with 24 different possible values of angles, yielding $|\mathcal{Y}_i| = 80 \times 80 \times 24 = 153,600$ possible placements.

Given a part configuration, we define cliques over pairwise and unary terms:

$$\theta(x, y) = \sum_{ij} \theta_{ij}^T \mathbf{f}_{ij}(x, y_i, y_j) + \sum_i \theta_i^T \mathbf{f}_i(x, y_i) \quad (26)$$

Thus, the parameters of the model are the pairwise and unary weight vectors θ_{ij} and θ_i corresponding to the pairwise and unary feature vectors $\mathbf{f}_{ij}(x, y_i, y_j)$ and $\mathbf{f}_i(x, y_i)$.

One of the reasons pictorial structures models have been so popular in the literature is that Felzenszwalb and Huttenlocher (2005) proposed a way to perform max inference on (26) in linear time using distance transforms, which is only possible if the pairwise term is a quadratic function of the displacement between neighbors y_i and y_j . We wish to go beyond such a simple geometric prior for the pairwise term of (26), and thus rely on standard $O(|\mathcal{Y}_i|^2)$ dynamic programming techniques to compute the MAP assignment or part posteriors, as was the case for linear-chain models in the previous section. However, unlike linear-chain models, many highly-effective pairwise features one might design would be intractable to compute in this manner for a reasonably-sized state space—for example an 80×80 image with a part angle discretization of 24 bins yields $|\mathcal{Y}_i|^2 = 57.6$ billion part-part hypotheses, far too many to store in a dynamic programming table (e.g., Figure 3).

6.2.1 Coarse-to-Fine Resolution Cascade

To overcome the issue of feature intractability, we define a *coarse-to-fine* structured prediction cascade over the resolution of the state space \mathcal{Y}_i (Figure 2b). Note that unlike the linear-chain cascade, the cliques do not change from one level to the next. Instead, the state space \mathcal{Y}_i of each part in one model is subdivided to form the state space of the next model. Once again, we learn

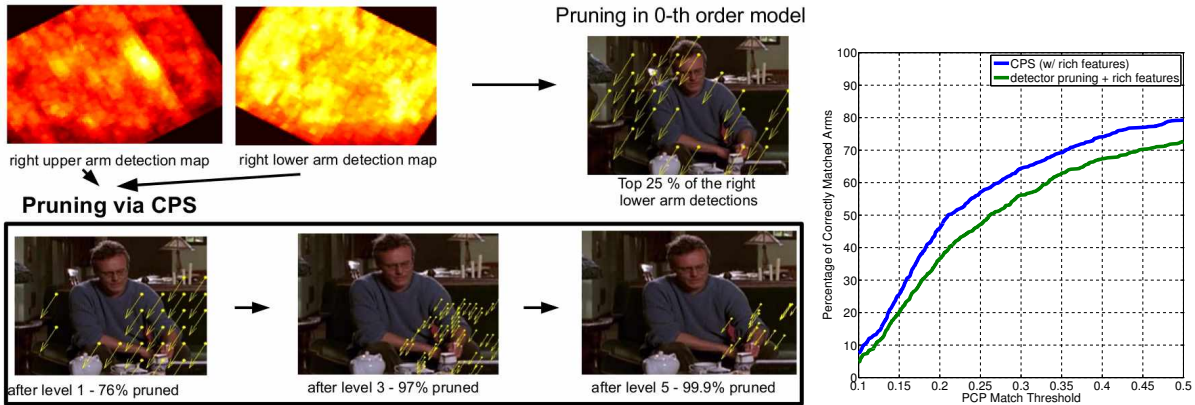


Figure 9: **Left:** Detector-based pruning (0th order model) by thresholding yields many hypotheses far way from the true one for the lower right arm. The CPS (bottom row), however, exploits global information to perform better pruning. **Right:** PCP curves of our cascade method (blue) show increased accuracy versus a detection pruning approach (green), evaluated using PCP on arm parts.

parameters θ and α for the cascade using Algorithm 1. The coarse-to-fine cascade is outlined in Figure 8.

Max-marginals for the pose model can be visualized to provide some intuition for max marginals. In general, the max-marginal for location/angle $\theta^*(x, y_i)$ is the score of the best global body pose which constrains $Y_i = y_i$. In a pictorial structure model, this corresponds to fixing limb i at (location, angle) y_i , and determining the highest scoring configuration of other part locations and angles under this constraint. Thus, a part could have weak individual image evidence of being at location y_i but still have a high max-marginal score if the rest of the model believes this is a likely location.

While the fine-level, target state space has size $80 \times 80 \times 24$, the first level cascade coarsens the state-space down to $10 \times 10 \times 12 = 1200$ states per part, which allows for efficient exhaustive inference. In our experiments, we always set $\alpha = 0$, effectively throwing away half of the states at each stage. After pruning we double one of the dimensions (first angle, then the minimum of width or height) and continue (see Table 3).

The coarse-to-fine stages use standard PS features. HoG part detectors are run once over the original state space, and the outputs are resized for features in the coarser state spaces. For pairwise features, we use the standard relative geometric cues of angle and displacement. The features are discretized uniformly, and thus multi-modal pairwise costs can be learned.

Once the cascade has reduced the fine-level state space to a manageable size, we apply a boosted model with many expensive, powerful features. As can be seen in Table 3, the coarse-to-fine cascade leaves us with roughly 500 valid assignments per part; for each possible part location and valid part pairs, we compute features using image contours, moments of the shape and regions underlying each part, color and texture appearance models, χ^2 color similarity between parts, and geometry.

One practical detail differentiates this cascade from others discussed in this section. Rather than learn a standard structured perceptron for prediction in the final stage, we concatenate all unary and pairwise features for part-pairs into a feature vector and learn boosting ensembles which give us our pairwise clique scores³. This method of learning clique scores has several advantages over stochastic subgradient learning: it is faster to train, can determine better thresholds on features

³ We use OpenCV's implementation of Gentleboost and boost on trees of depth 3, setting the optimal number of rounds via a hold-out set.

level	state dimensions	# states in the		state space reduction %	PCP _{0.2} arms oracle
		original space	pruned space		
0	10x10x12	153600	1200	00.00	—
1	10x10x24	72968	1140	52.50	54
3	20x20x24	6704	642	95.64	51
5	40x40x24	2682	671	98.25	50
7	80x80x24	492	492	99.67	50
detection pruning	80x80x24	492	492	99.67	44

Table 3: For each level of the cascade we present the reduction of the size of the state space after pruning each stage and the quality of the retained hypotheses measured using PCP_{0.2}. As a baseline, we compare to pruning the same number of states in the HoG detection map (see text).

than uniform binning, and can combine different features in a tree to learn complex, non-linear interactions. In general, we can use any method of learning with sparse inference for the final stage of Algorithm 1.

6.2.2 Buffy and PASCAL Dataset Results

We evaluated the pose cascade on the publicly available Buffy The Vampire Slayer v2.1 and PASCAL Stickmen datasets (Eichner. and Ferrari, 2009). We used the upper body detection windows provided with the dataset as input to localize and scale normalize the images before running our experiments as in Eichner. and Ferrari (2009); Ferrari et al. (2008); Andriluka et al. (2009). The standard 235 Buffy test images were used for testing, as well as the 360 detected people from PASCAL stickmen. We used the remaining 513 images from Buffy for training and validation.

The typical measure of performance on this dataset is a matching criteria based on both endpoints of each part (e.g., matching the elbow and the wrist correctly): A limb guess is correct if the limb endpoints are on average within r of the corresponding groundtruth segments, where r is a fraction of the groundtruth part length. By varying r , a performance curve is produced where the performance is measured in the percentage of correct parts (PCP) matched with respect to r . We define PCP _{r} as the value of the curve at r .

As shown in Table 4, the cascade performs comparably with the state-of-the-art on all parts, significantly outperforming earlier work. We also compared to a much simpler approach, inspired by Felzenszwalb et al. (2010) (detector pruning + rich features): We prune by thresholding each unary detection map individually to obtain the same number of states as in our final cascade level, and then apply our final model with rich features on these states. As can be seen in Figure 9, this baseline performs significantly worse than our method (performing about as well as a standard PS model as reported in Sapp et al. (2010a)). This makes a strong case for using max-marginals (e.g., a global image-dependent quantity) for pruning, as well as learning how to prune safely and efficiently, rather than using static thresholds on individual part scores as in Felzenszwalb et al. (2010).

In Table 3, we evaluate the test time efficiency and accuracy of our system after each successive stage of pruning. In the early stages, the state space is too coarse for the MAP state sequence of one of the pruning models to be meaningfully compared to the fine-resolution groundtruth, so we report PCP scores of the best possible as-yet unpruned state left in the original space. We choose a tight PCP_{0.2} threshold to get an accurate understanding of whether or not we have lost well-localized limbs. As seen in Table 3, the drop in PCP_{0.2} is small and linear, whereas the pruning of the state space is exponential—half of the states are pruned in the first stage. As a baseline,

Method	Torso	Head	Upper Arms	Lower Arms	Total
Buffy					
Andriluka et al. (2009)	90.7	95.5	79.3	41.2	73.5
Eichner. and Ferrari (2009)	98.7	97.9	82.8	59.8	80.1
Sapp et al. (2010a)	100	100	91.1	65.7	85.9
CPS (ours)	99.6	98.7	91.9	64.5	85.2
Detector pruning	99.6	87.3	90.0	55.3	79.6
PASCAL stickmen					
Eichner. and Ferrari (2009)	97.22	88.60	73.75	41.53	69.31
Sapp et al. (2010a)	100	98.0	83.9	54.0	79.0
CPS (ours)	100	99.2	81.5	53.9	78.3

Table 4: Comparison to other methods at $PCP_{0.5}$. See text for details. We perform comparably to state-of-the-art on all parts, improving on upper arms. (**NOTE:** the numbers included here are slightly different from the published version—what is seen here exactly matches the publicly available reference implementation at <http://vision.grasp.upenn.edu/video/>).

we evaluate the simple detector-based pruning described above. This leads to a significant loss of correct hypotheses, to which we attribute the poor end-system performance of this baseline (in Figure 9 and Table 4), even after adding richer features.

6.3 Loopy Graphs with Ensemble-SPC

We evaluated Ensemble-SPC in two experiments. First, we analyzed the “best-case” filtering performance of the summed max-marginal approximation to the true marginals on a synthetic image segmentation task, assuming the true scoring function $\theta(x, y)$ is available for inference. Second, we evaluated the real-world accuracy of our approach on a difficult, real-world human pose dataset (VideoPose). In both experiments, the max-marginal ensemble outperforms state-of-the-art baselines.

6.3.1 Asymptotic Filtering Accuracy on Synthetic Data

We first evaluated the filtering accuracy of the max-marginal ensemble on a synthetic 8-class segmentation task. For this experiment, we removed variability due to parameter estimation and focused our analysis on accuracy of inference. We compared our approach to Loopy Belief Propagation (Loopy BP) (Pearl, 1988; McEliece et al., 1998; Murphy et al., 1999), on a 11×11 two-dimensional grid MRF.⁴ For the ensemble, we used 22 unique “comb” tree structures to approximate the full grid model. To generate a synthetic instance, we generated unary potentials $\omega_i(k)$ uniformly on $[0, 1]$ and pairwise potentials log-uniformly: $\omega_{ij}(k, k') = e^{-v}$, where $v \sim \mathcal{U}[-25, 25]$ was sampled independently for every edge and every pair of classes. (Note that for the ensemble, we normalized unary and edge potentials by dividing by the number of times that each potential was included in any model.) It is well known that inference for such grid MRFs is generally difficult (Koller and Friedman, 2009), and we observed that Loopy BP failed to converge for at least a few variables on most examples we generated.

We evaluated our approach on 100 synthetic grid MRF instances. For each instance, we computed the accuracy of filtering using marginals from Loopy BP, the ensemble, and each individual

⁴We used the UGM Matlab Toolbox by Mark Schmidt for the Loopy BP and Gibbs MCMC comparisons, see: <http://people.cs.ubc.ca/~schmidtm/Software/UGM.html>.

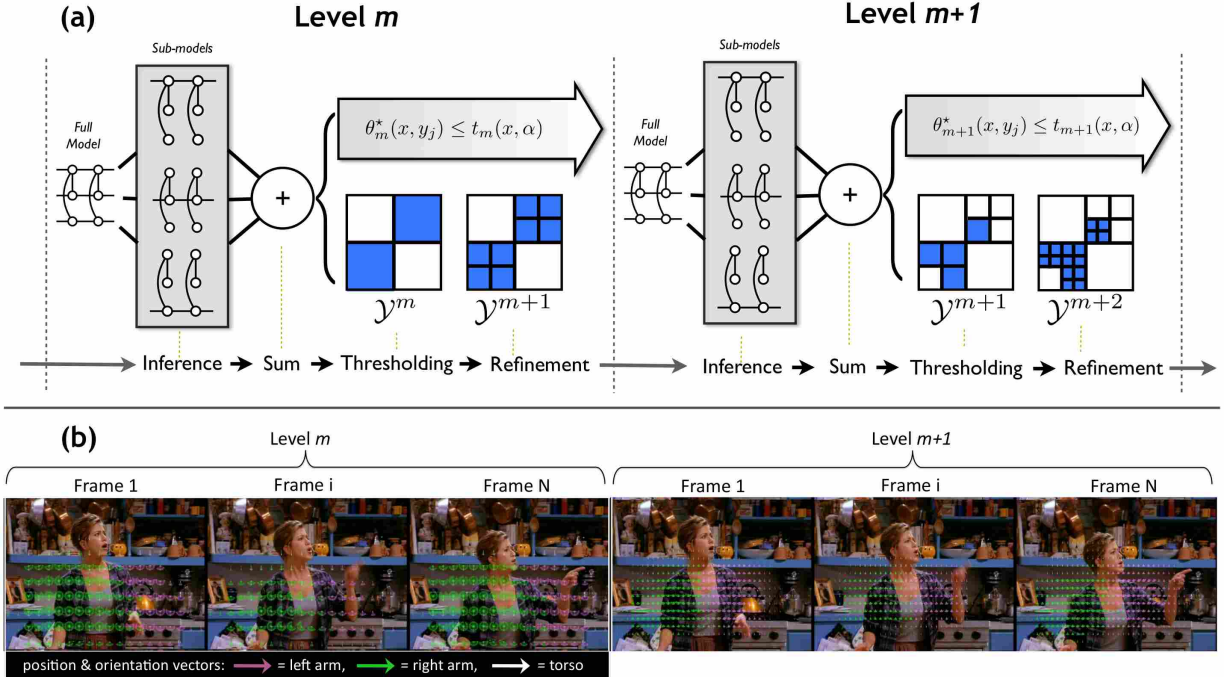


Figure 10: (a) Schematic overview Ensemble-SPC for human pose tracking. The m 'th level of the cascade takes as input a sparse set of states \mathcal{Y}^m for each variable y_j . The full model is decomposed into constituent sub-models (above, the three tree models used in the pose tracking experiment) and sparse inference is run. Next, the max marginals of the sub-models are summed to produce a single max marginal for each variable assignment: $\theta^*(x, y_j) = \sum_p \theta_p^*(x, y_j)$. Note that each level and each constituent model will have different parameters as a result of the learning process. Finally, the state spaces are thresholded based on the max-marginal scores and low-scoring states are filtered. Each state is then refined according to a state hierarchy (e.g., spatial resolution, or semantic categories) and passed to the next level of the cascade. This process can be repeated as many times as desired. In (b), we illustrate two consecutive levels of the ensemble cascade on real data, showing the filtered hypotheses left for a single video example.

sub-model. We determined error rates by counting the number of times “ground truth” was incorrectly filtered if the top K states were kept for each variable, where we sampled 1000 “ground truth” examples from the true joint distribution using Gibbs sampling. To obtain a good estimate of the true marginals, we restarted the chain for each sample and allowed 1000 iterations of mixing time. The result is presented in Figure 11 for all possible values of K (filter aggressiveness.) We found that the ensemble outperformed Loopy BP and the individual sub-models by a significant margin for all K .

We next investigated the question of whether or not the ensembles were most accurate on variables for which the sub-models tended to agree. For each variable y_{ij} in each instance, we computed the mean pairwise Spearman correlation between the ranking of the 8 classes induced by the max marginals of each of the 22 sub-models. We found that complete agreement between all sub-models never occurred (the median correlation was 0.38). We found that sub-model agreement was significantly correlated ($p < 10^{-15}$) with the error of the ensemble for all values of K , peaking at $\rho = -0.143$ at $K = 5$. Thus, increased agreement predicted a decrease in error of the ensemble. We then asked the question: Does the effect of model agreement explain the *improvement* of the ensemble over Loopy BP? In fact, the improvement in error compared to Loopy BP was *not* correlated with sub-model agreement for any K (maximum $\rho = 0.0185$, $p < 0.05$). Thus, sub-model agreement

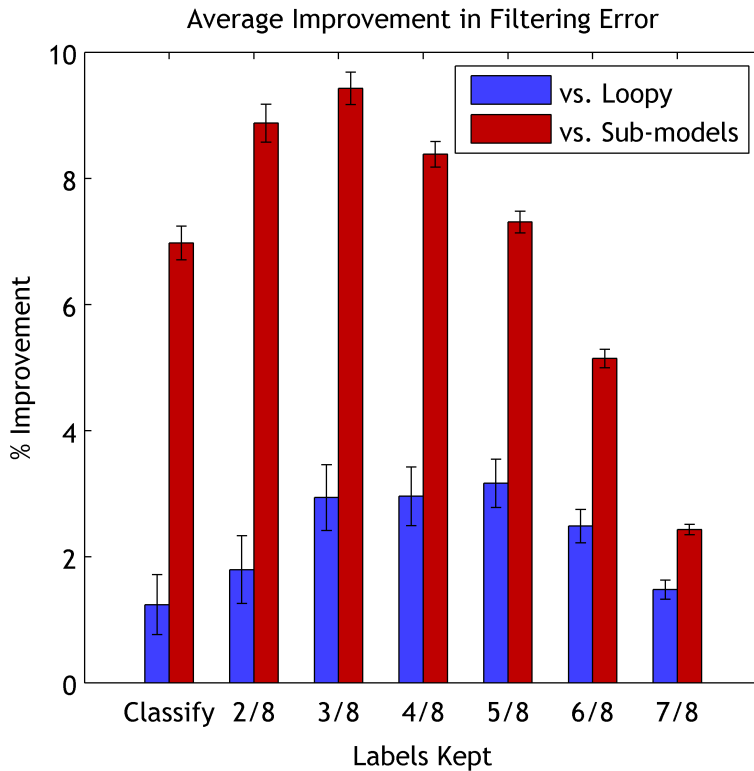


Figure 11: Improvement over Loopy BP and constituent tree-models on the synthetic segmentation task. Error bars show standard error.

does *not* explain the improvement over Loopy BP, indicating that sub-model disagreement is not related to the difficulty in inference problems that causes Loopy BP to underperform relative to the ensembles (e.g., due to convergence failure.)

6.3.2 Articulated Pose Tracking Cascade

The VideoPose dataset⁵ consists of 34 video clips of approximately 50 frames each. The clips were harvested from three popular TV shows: 3 from *Buffy the Vampire Slayer*, 27 from *Friends*, and 4 from *LOST*. Clips were chosen to highlight a variety of situations and movements when the camera is largely focused on a single actor. In our experiments, we use the *Buffy* and half of the *Friends* clips as training (17 clips), and the remaining *Friends* and *LOST* clips for testing. In total we test on 901 individual frames. The *Friends* are split so no clips from the same episode are used for both training and testing. We further set aside 4 of the *Friends* test clips to use as a development set. Each frame of each clip is hand-annotated with locations of joints of a full pose model; for simplicity, we use only the torso and upper arm annotations in this work, as these have the strongest continuity across frames and strong geometric relationships.

All of the models we evaluated on this dataset share the same basic structure: a variable for each limb’s (x, y) location and angle rotation (torso, left arm, and right arm) with edges between torso and arms to model pose geometry. We refer to this basic model, evaluated independently on each frame, as the “Single Frame” approach. For the VideoPose dataset, we augmented this model by adding edges between limb states in adjacent frames (Figure 10), forming an intractable, loopy

⁵The VideoPose dataset is available online at <http://vision.grasp.upenn.edu/video/>.

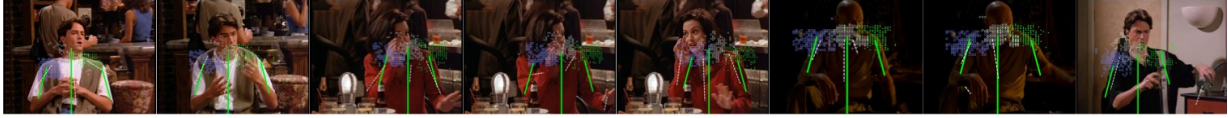


Figure 12: Qualitative test results. Points shown are the position of left/right shoulders and torsos at the last level of the ensemble SC (blue square, green dot, white circle resp.). Also shown (green line segments) are the best-fitting hypotheses to groundtruth joints, selected from within the top 4 max-marginal values. Shown as dotted gray lines is the best guess pose returned by the (Ferrari et al., 2008).

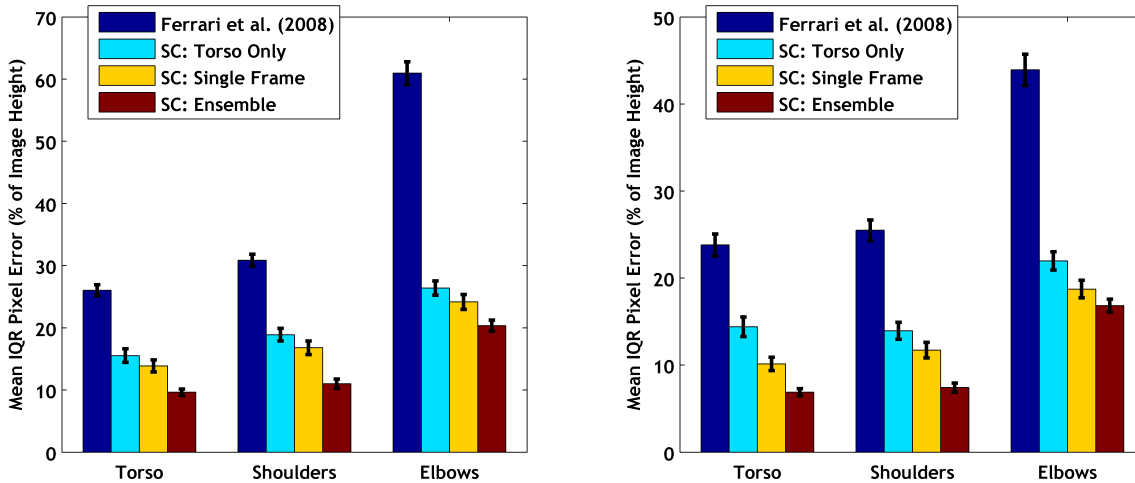
model. Our features in a single frame are the same as in the beginning levels of the pictorial structure cascade (Section 6.2): unary features are discretized Histogram of Gradient (HoG) part detectors scores, and pairwise terms measure relative displacement in location and angle between neighboring parts. Pairwise features connecting limbs across time also express geometric displacement, allowing our model to capture the fact that human limbs move smoothly over time.

We learned a coarse-to-fine structured cascade with six levels for tracking as follows. The six levels use increasingly finer state spaces for joint locations, discretized into bins of resolution 10×10 up to 80×80 , with each stage doubling one of the state space dimensions in the refinement step. All levels use an angular discretization of 24 bins. For the ensemble cascade, we learned three sub-models simultaneously (Figure 10), with each sub-model accounting for temporal consistency for a different limb by adding edges connecting the same limb in consecutive frames.

A summary of results are presented in Figure 13. We compared the single-frame cascade and the ensemble cascade to a state-of-the-art single-frame pose detector (Ferrari et al. (Ferrari et al., 2008)) and to one of the individual sub-models, modeling torso consistency only (“Torso Only”). We evaluated the method from (Ferrari et al., 2008) on only the first half of the test data due to computation time (taking approximately 7 minutes/frame). We found that the ensemble cascade was the most accurate for every joint in the model, that all cascades outperformed the state-of-the-art baseline, and, interestingly, that the single-frame cascade outperformed the torso-only cascade. We suspect that the poor performance of the torso-only model may arise because propagating only torso states through time leads to an over-reliance on the relatively weak torso signal to determine the location of all the limbs. Sample qualitative output from the ensemble is presented in Figure 12.

7 Conclusion

We presented Structured Prediction Cascades, a framework for adaptively increasing the complexity of structured models on a per-example basis while maintaining efficiency of inference. This allows for the construction and training of structured models of far greater complexity than was previously possible. We proposed two novel loss functions, filtering loss and efficiency loss, that measure the two objectives balanced by the cascade, and provided generalization bounds for these loss functions. We proposed a simple sub-gradient based learning algorithm to minimize these losses, and presented a stage-wise learning algorithm for the entire cascade in Algorithm 1. We also show how to extend the previous algorithm and theoretical results to the setting in which exact inference is intractable, using Ensemble-SPC. Finally, we showed experimentally state-of-the-art performance across multiple domains.



(a) Decoding Error.

(b) Top $K = 4$ Error.

	<i>State</i>	$PCP_{0.25}$	<i>Efficiency</i>
<i>Level</i>	<i>Dimensions</i>	<i>in top $K=4$</i>	(%)
0	$10 \times 10 \times 24$	–	–
2	$20 \times 20 \times 24$	98.8	87.5
4	$40 \times 40 \times 24$	93.8	96.9
6	$80 \times 80 \times 24$	84.6	99.2

(c) Ensemble efficiency.

Figure 13: (a),(b): Prediction error for VideoPose dataset. Reported errors are the average distance from a predicted joint location to the true joint for frames that lie in the $[25,75]$ inter-quartile range (IQR) of errors. Error bars show standard errors computed with respect to clips. All SC models outperform (Ferrari et al., 2008); the “torso only” persistence cascade introduces additional error compared to a single-frame cascade, but adding arm dependencies in the ensemble yields the best performance. (c): Summary of test set filtering efficiency and accuracy for the ensemble cascade. $PCP_{0.25}$ measures Oracle % of correctly matched limb locations given unfiltered states; see (Sapp et al., 2010b) for more details.

A Proofs of Theorems 1 and 2

We first summarize the Rademacher and Gaussian complexity definitions and results from Bartlett and Mendelson (2002) required to prove the theorems.

Definition 6 (Rademacher and Gaussian complexities). *Let $H : \mathcal{X} \mapsto \mathbb{R}$ be a function class and x^1, \dots, x^n be n independent samples from a fixed distribution. Define the random variables:*

$$\hat{R}(H) = \mathbb{E}_\sigma \left[\sup_{h \in H} \left\| \frac{2}{n} \sum_{i=1}^n \sigma_i h(x^i) \right\| \middle| x^1, \dots, x^n \right], \quad (27)$$

$$\hat{G}(H) = \mathbb{E}_g \left[\sup_{h \in H} \left\| \frac{2}{n} \sum_{i=1}^n g_i h(x^i) \right\| \middle| x^1, \dots, x^n \right], \quad (28)$$

where $\sigma_i \in \pm 1$ are independent uniform and $g_i \in \mathbb{R}$ are independent standard Gaussian. Then $R(H) = \mathbb{E}[\hat{R}(H)]$ and $G(H) = \mathbb{E}[\hat{G}(H)]$ are the Rademacher and Gaussian complexities of H .

Consider a general loss function $\Phi(y, \mathbf{h}(x))$ where $\mathbf{h}(x) \in \mathbb{R}^m$ represents the prediction function. In our case, $\mathbf{h}(x)$ is vector of clique assignment scores $\theta^\top \mathbf{f}_c(x, y_c)$ of dimension $\sum_{c \in \mathcal{C}} |\mathcal{Y}_c|$, indexed by y_c (a clique and its assignment). This vector $\mathbf{h}(x)$ contains all the information needed to compute the max-marginals and threshold for a given example x . Both \mathcal{L}_e and \mathcal{L}_f can be written in this general form, as we detail below.

Definition 7 (Lipschitz continuity with respect to Euclidean norm). *Let $\phi : \mathbb{R}^m \mapsto \mathbb{R}$, then ϕ is Lipschitz continuous with constant $L(\phi)$ with respect to Euclidean norm if for any $\mathbf{z}_1, \mathbf{z}_2 \in \mathbb{R}^m$:*

$$|\phi(\mathbf{z}_1) - \phi(\mathbf{z}_2)| \leq L(\phi) \|\mathbf{z}_1 - \mathbf{z}_2\|_2. \quad (29)$$

We recall the relevant results in the following theorem:

Theorem 3 (Bartlett and Mendelson, 2002). *Consider a loss function $\Phi : \mathcal{Y} \times \mathbb{R}^m \mapsto \mathbb{R}$ and a dominating cost function $\phi : \mathcal{Y} \times \mathbb{R}^m \mapsto \mathbb{R}$ such that $\Phi(y, \mathbf{z}) \leq \phi(y, \mathbf{z})$. Let $H : \mathcal{X} \mapsto \mathbb{R}^m$ be a vector-valued class of functions. Then for any integer n and any $0 < \delta < 1$, with probability $1 - \delta$ over samples of length n , every \mathbf{h} in H satisfies*

$$\mathbb{E}[\Phi(Y, \mathbf{h}(X))] \leq \hat{\mathbb{E}}[\phi(Y, \mathbf{h}(X))] + R_n(\tilde{\phi} \circ H) + \sqrt{\frac{8 \ln(2/\delta)}{n}}, \quad (30)$$

where $\tilde{\phi} \circ H$ is a class of functions defined by centered composition of ϕ with $\mathbf{h} \in H$, $\tilde{\phi} \circ \mathbf{h} = \phi(y, \mathbf{h}(x)) - \phi(y, 0)$.

Furthermore, Rademacher complexity can be bounded using Gaussian complexity: there are absolute constants c and C such that for every class H and every integer n ,

$$cR_n(H) \leq G_n(H) \leq (C \ln n)R_n(H). \quad (31)$$

Let $H : \mathcal{X} \rightarrow \mathbb{R}^m$ be a class of functions that is the direct sum of real-valued classes H_1, \dots, H_m . Then, for every integer n and every sample (x^1, \dots, x^n) ,

$$\hat{G}_n(\phi \circ H) \leq 2L(\phi) \sum_{i=1}^m \hat{G}_n(H_i), \quad (32)$$

where $L(\phi)$ is the Lipschitz constant of ϕ with respect to Euclidean distance. Finally, for the 2-norm-bounded linear class of functions, $H = \{x \mapsto \theta^\top \mathbf{f}(x) \mid \|\theta\|_2 \leq B, \|\mathbf{f}(x)\|_2 \leq 1\}$,

$$\hat{G}_n(H) \leq \frac{2B}{\sqrt{n}}. \quad (33)$$

A.1 Proof of Theorem 1

We will express our loss functions \mathcal{L}_e and \mathcal{L}_f and dominating loss functions \mathcal{L}_e^γ and \mathcal{L}_f^γ , in the in terms of the framework above. We reproduce the definitions side-by-side in a slightly modified form below, where $m = \sum_{c \in \mathcal{C}} |\mathcal{Y}_c|$ and the γ -margin step-function dominates the step-function $r_\gamma(z) \geq \mathbf{1}[z \leq 0]$ by construction:

$$\mathcal{L}_f(x, y; \theta, \alpha) = \mathbf{1}[\theta(x, y) - \tau(x; \theta, \alpha) \leq 0], \quad (34)$$

$$\mathcal{L}_f^\gamma(x, y; \theta, \alpha) = r_\gamma(\theta(x, y) - \tau(x; \theta, \alpha)), \quad (35)$$

$$\mathcal{L}_e(x, y; \theta, \alpha) = \frac{1}{m} \sum_{c \in \mathcal{C}, y_c \in \mathcal{Y}_c} \mathbf{1}[\tau(x; \theta, \alpha) - \theta^*(x, y_c) \leq 0], \quad (36)$$

$$\mathcal{L}_e^\gamma(x, y; \theta, \alpha) = \frac{1}{m} \sum_{c \in \mathcal{C}, y_c \in \mathcal{Y}_c} r_\gamma(\tau(x; \theta, \alpha) - \theta^*(x, y_c)). \quad (37)$$

We “vectorize” our scoring function θ and assignments y by defining vector-valued functions, where the vectors are indexed by clique assignments, y_c , with total dimension m .

Definition 8 (Vectorization).

$$\mathbf{h}_{y_c}(x) \triangleq \theta^\top \mathbf{f}_c(x, y_c) \quad (38)$$

$$\mathbf{v}_{y_c}(y') \triangleq \mathbf{1}[y'_c = y_c] \quad (39)$$

$$\theta(x, y) = \mathbf{h}(x)^\top \mathbf{v}(y) \quad (40)$$

Clearly, the m -dimensional vector $\mathbf{h}(x)$ contains all the information needed to compute the max-marginals and threshold for a given example x (we assume α is fixed). Hence we can define the losses in the form of Theorem 3:

$$\Phi_f(y, \mathbf{h}(x)) = \mathcal{L}_f(x, y; \theta, \alpha) \quad (41)$$

$$\phi_f(y, \mathbf{h}(x)) = \mathcal{L}_f^\gamma(x, y; \theta, \alpha) \quad (42)$$

$$\Phi_e(y, \mathbf{h}(x)) = \mathcal{L}_e(x, y; \theta, \alpha) \quad (43)$$

$$\phi_e(y, \mathbf{h}(x)) = \mathcal{L}_e^\gamma(x, y; \theta, \alpha) \quad (44)$$

What remains is to calculate the Lipschitz constants of ϕ_f and ϕ_e .

Theorem 4. $\phi_f(y, \cdot)$ and $\phi_e(y, \cdot)$ are Lipschitz (with respect to Euclidean distance on \mathbb{R}^m) with constant $\sqrt{2|\mathcal{C}|}/\gamma$ for all $y \in \mathcal{Y}$.

To prove Theorem 4, we bound Lipschitz constants of constituent functions of ϕ_f and ϕ_e .

Lemma 4. Fix any $y \in \mathcal{Y}$ and let $\phi_1 : \mathbb{R}^m \mapsto \mathbb{R}$ be defined as

$$\phi_1(\mathbf{z}) = \mathbf{z}^\top \mathbf{v}(y) - \max_{y' \in \mathcal{Y}} \mathbf{z}^\top \mathbf{v}(y').$$

Then $\phi_1(\mathbf{z}_1) - \phi_1(\mathbf{z}_2) \leq \sqrt{2|\mathcal{C}|} \|\mathbf{z}_1 - \mathbf{z}_2\|_2$ for any $\mathbf{z}_1, \mathbf{z}_2 \in \mathbb{R}^m$.

Proof. For brevity of notation in the proof below, we define $\mathbf{v} = \mathbf{v}(y)$, $\mathbf{v}_1 = \mathbf{v}(\operatorname{argmax}_{y'} \mathbf{z}_1^\top \mathbf{v}(y'))$ and $\mathbf{v}_2 = \mathbf{v}(\operatorname{argmax}_{y'} \mathbf{z}_2^\top \mathbf{v}(y'))$, with ties broken arbitrarily but deterministically. Then,

$$\begin{aligned} \phi_1(\mathbf{z}_1) - \phi_1(\mathbf{z}_2) &= \mathbf{z}_1^\top \mathbf{v} - \mathbf{z}_1^\top \mathbf{v}_1 - \mathbf{z}_2^\top \mathbf{v} + \mathbf{z}_2^\top \mathbf{v}_2 \\ &= (\mathbf{z}_2 - \mathbf{z}_1)^\top (\mathbf{v}_2 - \mathbf{v}) + \mathbf{z}_1^\top (\mathbf{v}_2 - \mathbf{v}_1) \\ &\leq (\mathbf{z}_2 - \mathbf{z}_1)^\top (\mathbf{v}_2 - \mathbf{v}) \\ &\leq \|\mathbf{z}_2 - \mathbf{z}_1\|_2 \|\mathbf{v}_2 - \mathbf{v}\|_2 \\ &\leq \sqrt{2|\mathcal{C}|} \|\mathbf{z}_1 - \mathbf{z}_2\|_2. \end{aligned}$$

The last three steps follow (1) from the fact that \mathbf{v}_1 maximizes $\mathbf{z}_1^\top \mathbf{v}(y')$ (so that $\mathbf{z}_1^\top (\mathbf{v}_2 - \mathbf{v}_1)$ is negative), (2) from the Cauchy-Schwarz inequality, and (3) from the fact that there are $|\mathcal{C}|$ cliques, each of which can contribute at most a single non-zero entry in \mathbf{v} or \mathbf{v}_2 . \square

Lemma 5. Fix any $y \in \mathcal{Y}$ and let $\phi_2 : \mathbb{R}^m \mapsto \mathbb{R}$ be defined as

$$\phi_2(\mathbf{z}) = \mathbf{z}^\top \mathbf{v}(y) - \frac{1}{m} \sum_{c \in \mathcal{C}, y'_c \in \mathcal{Y}_c} \max_{y'' : y''_c = y'_c} \mathbf{z}^\top \mathbf{v}(y'').$$

Then $\phi_2(\mathbf{z}_1) - \phi_2(\mathbf{z}_2) \leq \sqrt{2|\mathcal{C}|} \|\mathbf{z}_1 - \mathbf{z}_2\|_2$ for any $\mathbf{z}_1, \mathbf{z}_2 \in \mathbb{R}^m$.

Proof. Let $\mathbf{v} = \mathbf{v}(y)$, $\mathbf{v}_{1y'_c} = \mathbf{v}(\operatorname{argmax}_{y'' : y''_c = y'_c} \mathbf{z}_1^\top \mathbf{v}(y''))$ and $\mathbf{v}_{2y'_c} = \mathbf{v}(\operatorname{argmax}_{y'' : y''_c = y'_c} \mathbf{z}_2^\top \mathbf{v}(y''))$.

$$\begin{aligned} \phi_2(\mathbf{z}_1) - \phi_2(\mathbf{z}_2) &= \frac{1}{m} \sum_{c \in \mathcal{C}, y'_c \in \mathcal{Y}_c} \mathbf{z}_1^\top \mathbf{v} - \mathbf{z}_1^\top \mathbf{v}_{1y'_c} - \mathbf{z}_2^\top \mathbf{v} + \mathbf{z}_2^\top \mathbf{v}_{2y'_c} \\ &= \frac{1}{m} \sum_{c \in \mathcal{C}, y'_c \in \mathcal{Y}_c} (\mathbf{z}_2 - \mathbf{z}_1)^\top (\mathbf{v}_{2y'_c} - \mathbf{v}) + \mathbf{z}_1^\top (\mathbf{v}_{2y'_c} - \mathbf{v}_{1y'_c}) \\ &\leq \frac{1}{m} \sum_{c \in \mathcal{C}, y'_c \in \mathcal{Y}_c} (\mathbf{z}_2 - \mathbf{z}_1)^\top (\mathbf{v}_{2y'_c} - \mathbf{v}) \\ &\leq \frac{1}{m} \sum_{c \in \mathcal{C}, y'_c \in \mathcal{Y}_c} \sqrt{2|\mathcal{C}|} \|\mathbf{z}_1 - \mathbf{z}_2\|_2 = \sqrt{2|\mathcal{C}|} \|\mathbf{z}_1 - \mathbf{z}_2\|_2. \end{aligned}$$

The inequalities follow using a similar argument to previous lemma, but made separately for each y'_c . \square

Lemma 6. Fix any $y \in \mathcal{Y}$ and let

$$\phi_3(\mathbf{z}) = \alpha \phi_1(\mathbf{z}) + (1 - \alpha) \phi_2(\mathbf{z}) = \overbrace{\mathbf{z}^\top \mathbf{v}(y)}^{\theta(x,y)} - \overbrace{\left(\alpha \max_{y'} \mathbf{z}^\top \mathbf{v}(y') + \frac{1 - \alpha}{m} \sum_{y'_c} \max_{y'' : y''_c = y'_c} \mathbf{z}^\top \mathbf{v}(y'') \right)}^{\tau(x;\theta,\alpha)},$$

where the over-braces show the relationship to the score of the correct label sequence and the threshold, assuming $\mathbf{z} = \mathbf{h}(x)$. Then $\phi_3(\mathbf{z}_1) - \phi_3(\mathbf{z}_2) \leq \sqrt{2|\mathcal{C}|} \|\mathbf{z}_1 - \mathbf{z}_2\|_2$ for any $\mathbf{z}_1, \mathbf{z}_2 \in \mathbb{R}^m$ and the Lipschitz constant of $\phi_f = r_\gamma \circ \phi_3$ is bounded by $\sqrt{2|\mathcal{C}|}/\gamma$.

Proof. Combining two previous lemmas we have that

$$\phi_3(\mathbf{z}_1) - \phi_3(\mathbf{z}_2) = \alpha(\phi_1(\mathbf{z}_1) - \phi_1(\mathbf{z}_2)) + (1 - \alpha)(\phi_2(\mathbf{z}_1) - \phi_2(\mathbf{z}_2)) \leq \sqrt{2|\mathcal{C}|} \|\mathbf{z}_1 - \mathbf{z}_2\|_2.$$

To show that ϕ_f is Lipschitz continuous with constant $\sqrt{2|\mathcal{C}|}/\gamma$, we note that $\phi_f = r_\gamma \circ \phi_3$ so $L(\phi_f) = L(r_\gamma) \cdot L(\phi_3) \leq \sqrt{2|\mathcal{C}|}/\gamma$. \square

Next, we show that ϕ_e is Lipschitz continuous with the same constant.

Lemma 7. Fix $c \in \mathcal{C}$ and $y_c \in \mathcal{Y}$ and let $\phi_{[y_c]} : \mathbb{R}^m \mapsto \mathbb{R}$ be defined as

$$\phi_{[y_c]}(\mathbf{z}) = \overbrace{\left(\max_{y': y'_c = y_c} \mathbf{z}^\top \mathbf{v}(y') \right)}^{\theta^*(x, y_c)} - \overbrace{\left(\alpha \max_{y'} \mathbf{z}^\top \mathbf{v}(y') + \frac{1-\alpha}{m} \sum_{y'_c} \max_{y'': y''_c = y'_c} \mathbf{z}^\top \mathbf{v}(y'') \right)}^{\tau(x; \theta, \alpha)},$$

where the over-braces show the relationship to max-marginal of y_c and the threshold and, assuming $\mathbf{z} = \mathbf{h}(x)$. Then $\phi_{[y_c]}(\mathbf{z}_1) - \phi_{[y_c]}(\mathbf{z}_2) \leq \sqrt{2|\mathcal{C}|} \|\mathbf{z}_1 - \mathbf{z}_2\|_2$ for any $\mathbf{z}_1, \mathbf{z}_2 \in \mathbb{R}^m$.

Proof. We once again apply the trick from the proof of Lemma 4. Let

$$\begin{aligned} \mathbf{v}_1 &= \mathbf{v}(\operatorname{argmax}_{y'} \mathbf{z}_1^\top \mathbf{v}(y')), & \mathbf{v}_2 &= \mathbf{v}(\operatorname{argmax}_{y'} \mathbf{z}_2^\top \mathbf{v}(y')), \\ \mathbf{v}_{1y'_c} &= \mathbf{v}(\operatorname{argmax}_{y'': y''_c = y'_c} \mathbf{z}_1^\top \mathbf{v}(y'')), & \mathbf{v}_{2y'_c} &= \mathbf{v}(\operatorname{argmax}_{y'': y''_c = y'_c} \mathbf{z}_2^\top \mathbf{v}(y'')). \end{aligned}$$

Then, we have:

$$\begin{aligned} \phi_{[y_c]}(\mathbf{z}_1) - \phi_{[y_c]}(\mathbf{z}_2) &= (\mathbf{z}_1^\top \mathbf{v}_{1y_c} - \mathbf{z}_2^\top \mathbf{v}_{2y_c}) + \alpha(\mathbf{z}_2^\top \mathbf{v}_2 - \mathbf{z}_1^\top \mathbf{v}_1) + \frac{1-\alpha}{m} \sum_{y'_c} (\mathbf{z}_2^\top \mathbf{v}_{2y'_c} - \mathbf{z}_1^\top \mathbf{v}_{1y'_c}) \\ &\leq (\mathbf{z}_1 - \mathbf{z}_2)^\top \mathbf{v}_{1y_c} + \alpha(\mathbf{z}_2 - \mathbf{z}_1)^\top \mathbf{v}_2 + \frac{1-\alpha}{m} \sum_{y'_c} (\mathbf{z}_2 - \mathbf{z}_1)^\top \mathbf{v}_{2y'_c} \\ &= \frac{1}{m} \sum_{y'_c} (\mathbf{z}_1 - \mathbf{z}_2)^\top \left(\mathbf{v}_{1y_c} - \alpha \mathbf{v}_2 - (1-\alpha) \mathbf{v}_{2y'_c} \right) \\ &\leq \frac{1}{m} \sum_j \sqrt{2|\mathcal{C}|} \|\mathbf{z}_1 - \mathbf{z}_2\|_2 = \sqrt{2|\mathcal{C}|} \|\mathbf{z}_1 - \mathbf{z}_2\|_2. \end{aligned}$$

Here once again we have condensed the argument similar to Lemma 4. □

Finally, we note that $\phi_e(\mathbf{z}) = 1/m \sum_i r_\gamma(\phi_{[y_c]}(\mathbf{z}))$. Therefore $L(\phi_e) = 1/m \sum_i \sqrt{2|\mathcal{C}|}/\gamma = \sqrt{2|\mathcal{C}|}/\gamma$, thus completing the proof of Theorem 4. Now turning back to Theorem 1, we note that the class of functions H we are working with is the direct sum of m linear classes each bounded by norm B . Hence we complete the proof of Theorem 1, by using Theorem 3, with $R_n(\tilde{\phi}_f \circ H) = R_n(\tilde{\phi}_e \circ H) \leq \frac{cmB\sqrt{|\mathcal{C}|}}{\gamma\sqrt{n}}$ for some constant c .

A.2 Proof of Theorem 2

We define

$$\begin{aligned} \Phi_{joint}(y, \mathbf{h}(x)) &\triangleq \mathcal{L}_{joint}(x, y; \theta, \alpha) = \mathbf{1} \left[\left(\sum_p \theta_p(x, y) - \tau(x; \theta_p, \alpha) \right) \leq 0 \right], \\ \phi_{joint}(y, \mathbf{h}(x)) &\triangleq \mathcal{L}_{joint}^\gamma(x, y; \theta, \alpha) = r_\gamma \left(\sum_p \theta_p(x, y) - \tau(x; \theta_p, \alpha) \right) \end{aligned}$$

Once again, we fix any $y \in \mathcal{Y}$ and for each p , let (similar to Lemma 6)

$$\phi_3(\mathbf{z}_p) = \overbrace{\mathbf{z}_p^\top \mathbf{v}(y)}^{\theta_p(x,y)} - \overbrace{\left(\alpha \max_{y'} \mathbf{z}_p^\top \mathbf{v}(y') + \frac{1-\alpha}{m} \sum_{y'_c} \max_{y''_c=y'_c} \mathbf{z}_p^\top \mathbf{v}(y'') \right)}^{\tau(x;\theta_p,\alpha)},$$

where the over-braces show the relationship to the score of the correct label sequence under model p and the threshold for model p , assuming $\mathbf{z}_p = \mathbf{h}_p(x)$ of model p .

Then $\phi_{joint}(y, \mathbf{h}(x)) = r_\gamma(\sum_p \phi_3(\sum_p \mathbf{z}_p))$ has Lipschitz constant $\sqrt{2|\mathcal{C}|}P/\gamma$, since we can apply Lemma 6 for each p , and $\phi_{joint}(y, \mathbf{h}(x)) = r_\gamma(\sum_p \theta_p(x, y) - \tau(x; \theta_p, \alpha))$ has Lipschitz constant at most $\sqrt{2|\mathcal{C}|}P/\gamma$ because if composition with r_γ and the sum of P identical terms. In Theorem 2, our function class H is the direct sum of $m * P$ linear classes each bounded by norm B/P , hence $R_n(\tilde{\phi}_{joint} \circ H) \leq \frac{cmPB\sqrt{|\mathcal{C}|}}{\gamma\sqrt{n}}$ for some constant c .

References

- A. Agarwal, J. Duchi, P. Bartlett, and C. Levrard. Oracle inequalities for computationally budgeted model selection. In *Proc. COLT*, 2011. 3
- H. Akaike. A new look at the statistical model identification. *Automatic Control, IEEE Transactions on*, 19(6):716 – 723, dec 1974. 1
- M. Andriluka, S. Roth, and B. Schiele. Pictorial structures revisited: People detection and articulated pose estimation. In *Proc. CVPR*, 2009. 17, 20, 21
- A. Barron, L. Birgé, and P. Massart. Risk bounds for model selection via penalization. *Probability theory and related fields*, 113(3):301–413, 1999. 1
- P. Bartlett and S. Mendelson. Rademacher and Gaussian complexities: Risk bounds and structural results. *JMLR*, 3:463–482, 2002. 14, 26
- P. L. Bartlett, S. Boucheron, and G. Lugosi. Model selection and error estimation. *Machine Learning*, 48:85–113, 2002. 1
- D. Bertsekas. *Nonlinear Programming*. Athena Scientific, second edition, 1999. 9
- L. Bottou and O. Bousquet. The tradeoffs of large scale learning. In *Neural Information Processing Systems*, pages 161–168, 2008. 3
- X. Carreras., M. Collins, and T. Koo. TAG, dynamic programming, and the perceptron for efficient, feature-rich parsing. In *Proc. CoNLL*, 2008. 3
- G. Cavallanti, N. Cesa-Bianchi, and C. Gentile. Tracking the best hyperplane with a simple budget Perceptron. *Machine Learning*, 69(2):143–167, 2007. 3
- E. Charniak. A maximum-entropy-inspired parser. In *Proc. NAACL*, 2000. 3
- D. Chiang, A. Lopez, N. Madnani, C. Monz, P. Resnik, and M. Subotin. The hiero machine translation system: extensions, evaluation, and analysis. In *Proc. HLT/EMNLP*, pages 779–786, Stroudsburg, PA, USA, 2005. Association for Computational Linguistics. 2

- K. Crammer, J. Kandola, and Y. Singer. Online classification on a budget. In *Proc. NIPS*. MIT Press, 2003. 3
- H. Daumé, J. Langford, and D. Marcu. Search-based structured prediction. *Machine Learning*, 75(3):297–325, 2009. URL <http://dx.doi.org/10.1007/s10994-009-5106-x>. 17
- O. Dekel, S. Shalev-Shwartz, and Y. Singer. The Forgetron: A kernel-based Perceptron on a budget. *SIAM Journal on Computing*, 37(5):1342–1372, 2008. 3
- L. Devroye, L. Györfi, and G. Lugosi. *A probabilistic theory of pattern recognition*, volume 31. Springer Verlag, 1996. 1
- M. Eichner. and V. Ferrari. Better appearance models for pictorial structures. In *Proc. BMVC*, 2009. 20, 21
- P. Felzenszwalb and D. Huttenlocher. Pictorial structures for object recognition. *IJCV*, 61(1):55–79, 2005. 17, 18
- P. Felzenszwalb, R. Girshick, and D. McAllester. Cascade object detection with deformable part models. In *Proc. CVPR*, 2010. 3, 4, 20
- V. Ferrari, M. Marin-Jimenez, and A. Zisserman. Progressive search space reduction for human pose estimation. In *Proc. CVPR*, 2008. 17, 20, 24, 25
- F. Fleuret and D. Geman. Coarse-to-fine face detection. *IJCV*, 41(1/2), 2001. 3, 4
- T. Gao and D. Koller. Active classification based on value of classifier. In *Proc. NIPS*, 2011. 3
- R. Kassel. *A Comparison of Approaches to On-line Handwritten Character Recognition*. PhD thesis, Massachusetts Institute of Technology, 1995. 15
- D. Koller and N. Friedman. *Probabilistic Graphical Models: Principles and Techniques*. The MIT Press, 2009. 21
- N. Komodakis, N. Paragios, and G. Tziritas. MRF optimization via dual decomposition: Message-passing revisited. In *Proc. ICCV*, 2007. 9
- J. Lafferty, A. McCallum, and F. Pereira. Conditional random fields: Probabilistic models for segmenting and labeling sequence data. In *Proc. ICML*, 2001. 2
- L. Lefakis and F. Fleuret. Joint cascade optimization using A product of boosted classifiers. In *Proc. NIPS*, 2010. 3
- C. L. Mallows. Some comments on C_p . *Technometrics*, 15(4):pp. 661–675, 1973. 1
- R.J. McEliece, D.J.C. MacKay, and J.F. Cheng. Turbo decoding as an instance of Pearl’s belief propagation algorithm. *J. on Selected Areas in Communications*, 16(2):140–152, 1998. 21
- K.P. Murphy, Y. Weiss, and M.I. Jordan. Loopy belief propagation for approximate inference: An empirical study. In *Proc. UAI*, pages 467–475, 1999. 21
- J. Pearl. *Probabilistic reasoning in intelligent systems: networks of plausible inference*. Morgan Kaufmann, 1988. 21

- S. Petrov. *Coarse-to-Fine Natural Language Processing*. PhD thesis, University of California at Bekeley, 2009. 3
- S. Petrov, A. Haghighi, and D. Klein. Coarse-to-fine syntactic machine translation using language projections. In *Proc. EMNLP*, pages 108–116, 2008. 2
- D. Ramanan and C. Sminchisescu. Training deformable models for localization. In *CVPR*, 2006. 17
- A. Rush and S. Petrov. Vine pruning for efficient multi-pass dependency parsing. In *Proc. NAACL*, 2012. 3
- B. Sapp, C. Jordan, and B. Taskar. Adaptive pose priors for pictorial structures. In *Proc. CVPR*, 2010a. 20, 21
- B. Sapp, A. Toshev, and B. Taskar. Cascaded models for articulated pose estimation. In *Proc. ECCV*, 2010b. 2, 4, 25
- S. Shalev-Shwartz and N. Srebro. SVM optimization: inverse dependence on training set size. In *International Conference on Machine learning*, pages 928–935, 2008. 3
- S. Shalev-Shwartz, Y. Singer, and N. Srebro. Pegasos: Primal estimated sub-gradient SOLver for SVM. In *Proc. ICML*, 2007. 13
- B. Taskar, C. Guestrin, and D. Koller. Max margin Markov networks. In *Proc. NIPS*, 2003. 15, 16
- V. Vapnik and A. Chervonenkis. *Theory of pattern recognition*. Nauka, 1974. 1
- A. Venugopal, A. Zollmann, and V. Stephan. An efficient two-pass approach to synchronous-CFG driven statistical MT. In *Proc. HLT-NAACL*, pages 500–507, 2007. 2
- P. Viola and M. Jones. Rapid object detection using a boosted cascade of simple features. In *Proc. CVPR*, 2001. 3, 4
- D. Weiss and B. Taskar. Structured prediction cascades. In *Proc. AISTATS*, 2010. 2
- D. Weiss, B. Sapp, and B. Taskar. Sidestepping intractable inference with structured ensemble cascades. In *Proc. NIPS*, 2010. 2, 9